

Kitaev Building-block Construction for Higher-order Topological Superconductors

Rui-Xing Zhang,^{1,*} Jay D. Sau,^{1,†} and S. Das Sarma¹

¹*Condensed Matter Theory Center and Joint Quantum Institute, Department of Physics,
University of Maryland, College Park, Maryland 20742-4111, USA*

(Dated: March 6, 2020)

We propose a general theoretical framework for both constructing and diagnosing symmetry-protected higher-order topological superconductors using Kitaev building blocks, a higher-dimensional generalization of Kitaev’s one-dimensional Majorana model. For a given crystalline symmetry, the Kitaev building blocks serve as a complete basis to construct all possible Kitaev superconductors that satisfy the symmetry requirements. Based on this Kitaev construction, we identify a simple but powerful bulk Majorana counting rule that can unambiguously diagnose the existence of higher-order topology for all Kitaev superconductors. For a systematic construction, we propose two inequivalent stacking strategies using the Kitaev building blocks and provide minimal tight-binding models to explicitly demonstrate each stacking approach. Notably, some of our Kitaev superconductors host higher-order topology that cannot be captured by the existing symmetry indicators in the literature. Nevertheless, our Majorana counting rule does enable a correct diagnosis for these “beyond-indicator” models. We conjecture that all Wannierizable superconductors should yield a decomposition in terms of our Kitaev building blocks, up to adiabatic deformations. Based on this conjecture, we propose a universal diagnosis of higher-order topology that possibly works for all Wannierizable superconductors. We also present a realistic example of higher-order topological superconductors with fragile Wannier obstruction to verify our conjectured universal diagnosis. Our work paves the way for a complete topological theory for superconductors.

CONTENTS

I. Introduction	1	2. $H_2(\mathbf{k})$ with $ t > m $: A Higher-order TSC	12
II. Main Results	3	3. $H_2(\mathbf{k})$ with $ t < m $: A Weak TSC	12
A. What is a Higher-order Topological Superconductor?	3	C. Displaced Stacking with Different Building Blocks	13
B. Kitaev Limit for Superconductors	4	1. Model Hamiltonian and Higher-order Topology	13
C. Condition of Higher-order Topology for Kitaev Superconductors	5	2. Beyond Symmetry Indicators	14
III. Classification of Kitaev Superconductors and Majorana Counting	5	V. A Conjecture of Universal Topological Diagnosis	15
A. Kitaev Building Blocks	6	VI. Application to a Realistic Higher-order Topological Superconductor	16
B. Polarization and Topological Classification for Kitaev Superconductors	6	A. Model Hamiltonian for Stacked Chiral TSCs	16
C. Atomic Site, Stacking, and Open Boundary Conditions	7	B. Higher-order Topology from a Boundary Perspective	16
D. The Majorana Counting Rule: A Derivation	8	C. Fragile Wannier Obstruction	17
IV. Building-block Construction of Higher-order TSCs	8	D. Nested Wilson Loop, Parity Data, and Majorana Counting	18
A. Face-to-face Stacking	9	VII. Conclusion	19
1. Recipe of Face-to-face Stacking	9	Acknowledgments	19
2. A Minimal Face-to-face Stacking Model with Higher-order Topology	9	References	20
B. Displaced Stacking with the Same Building Blocks	10		
1. A Minimal Double-Stacking Model with Higher-order Topology	11		

I. INTRODUCTION

The concept of topology has revolutionized our understanding of condensed matter systems in the past decades. The revolution started with the quantum Hall effect [1-3] and continued through the seminal works on

* ruixing@umd.edu
† jaydsau@umd.edu

the 10-fold way [4, 5] and topological insulators (TI) [6], becoming a dominant theme in condensed matter physics over the last 10 years, leading to the exciting concept of topological quantum computation using non-Abelian anyons [7, 8]. Even within the same symmetry class, there could exist several types of topologically distinct phases that cannot be connected through an adiabatic evolution path and thus behave differently in various aspects. In particular, the topological properties for a large class of systems are only well-defined when certain types of symmetries are present. This class of topological systems is known as the symmetry-protected topological (SPT) state [9–11], and most, if not all, currently known free-fermion topological states are technically SPT phases even if this is not always explicitly mentioned. When placed on an open geometry, the bulk topology of a D -dimensional SPT system enforces the existence of anomalous in-gap modes on its $(D - 1)$ -dimensional boundary, which cannot be removed without either closing the bulk energy gap or breaking the protection symmetry. Such in-gap boundary modes are “anomalous” in the sense that they can never be realized in any $(D - 1)$ -dimensional bulk system – they are strictly the boundary modes corresponding to the bulk topology, an example of a bulk-boundary correspondence.

For free-fermion SPT systems such as topological insulators, topological band theories are extremely successful in classifying and predicting new topological materials [12, 13]. To capture various band topology, one direct approach is to mathematically define the corresponding topological invariants for band insulators with different internal or crystalline symmetries [11, 14–19]. On the other hand, all known topological band insulators present obstruction to a symmetric and localized Wannier function description [20, 21]. Therefore, Wannierizability can be treated as a diagnosis for distinguishing topological and trivial band insulators. Notably, the recent breakthrough in the band representation theory provides us with a complete list of all possible trivial atomic insulators for all space groups [22]. Consequently, topological systems can be systematically sorted by simply excluding the known atomic limits for band insulators. This is, in principle, a conceptually revolutionary new way of classifying insulators, connecting quantum chemistry (i.e. the atomic limit) with solid state band theories.

It was recently realized that some topological insulators protected by lattice symmetries admit a higher-order version of the bulk-boundary correspondence [23], which are dubbed higher-order topological insulators [24–32]. Specifically, the D -dimensional bulk topology in these systems is indicated by anomalous in-gap modes on their $(D - n)$ -dimensional boundary with $n \in \{2, \dots, D - 1\}$. Some three-dimensional (3d) axion insulator candidates [33, 34], including EuIn_2As_2 [35], $\text{Bi}_{2-x}\text{Sm}_x\text{Se}_3$ [36], and $\text{MnBi}_{2n}\text{Te}_{3n+1}$ [37], have been theoretically proposed to host 1d inversion-protected chiral fermion channels that live on the “hinges” connecting two neighboring gapped surfaces. Meanwhile, experimental sig-

natures of 1d inversion-protected helical hinge modes have been observed in Bismuth using scanning tunneling microscopy [38]. Similar to a conventional TI, a higher-order TI is necessarily Wannier obstructed. As a result, by filtering out Wannierizable atomic insulators, researchers have designed/derived simple functions of crystalline symmetry eigenvalues at high-symmetry momenta, which can correctly diagnose the higher-order topology. These symmetry-eigenvalue-based functions are known as “symmetry indicators” [29, 39, 40].

In this work, our main focus is the higher-order version of topological superconductors (TSC), which has been recently under active research in the community [41–53]. In particular, a 2d higher-order TSC is featured by zero-dimensional (0d) corner-localized Majorana zero modes, which potentially offer new promising platforms for Majorana-based topological quantum computation [54, 55]. The great success for classifying band insulators inspires us to ask whether similar symmetry-based topological indicators could be defined to classify (higher-order) topology in superconductors.

Indeed, several groups have independently developed similar proposals for symmetry indicators for classifying higher-order TSCs [56–62]. However, it is notable that these symmetry-indicator-based classifications usually require a constant representation of a certain symmetry (e.g. inversion symmetry), which cannot always be fulfilled for a general superconducting system described by Bogoliubov-de Gennes (BdG) equations with sublattice degrees of freedom. While this limitation casts doubt on the completeness of any symmetry-eigenvalue-based classification schemes (since the applicability of such a scheme beyond insulators is apparently not obvious), we are not aware of any efforts towards finding possible “beyond-indicator” models. Nevertheless, we do believe that such an effort is necessary, crucial, and urgent in this field, because the beyond-indicator models manifest themselves as a touchstone for checking the “*completeness*” of any proposed topological classification schemes for higher-order TSCs.

On the other hand, several important conceptual caveats and difficulties remain to be elucidated in this field, particularly in the context of superconductors. First of all, the physical meaning of being “atomic” for a superconductor is unclear. As is known, the most important length scale for superconductors is the superconducting coherence length ξ , which is about $10^1 \sim 10^3$ atomic lattice constants. This directly implies that the atomic-scale microscopic physics should not be crucial for describing superconductivity and its related topological phenomena. In other words, any topology-enforced Majorana physics for a topological superconductor (TSC) should just arise from the low-energy physics near the Fermi surface, where the energy cut-off is around ξ^{-1} and not a microscopic atomic lattice length scale. This feature clearly distinguishes between the physical meanings of “atomic limit” for superconductors and insulators.

Second, while the trivality of atomic band insulators

can be diagnosed from its Wannierizability, the conventional wisdom indicates that *a Wannierizable superconductor can also be topological*. As perhaps the simplest example, the 1d Kitaev Majorana chain [7] is not only Wannierizable but also hosting 0d Majorana end modes. Clearly, the 0d Majorana modes are anomalous boundary modes and cannot be realized in any 0d electron systems. Therefore, it is natural to speculate that a 2d higher-order topological superconductor with 0d Majorana corner modes could also be Wannierizable, similar to a Kitaev chain [7].

Motivated by the above considerations, we present in this work a general framework of constructing and diagnosing 2d Wannierizable higher-order TSCs. In particular, we define the *Kitaev limit* as a direct higher-dimensional generalization for Kitaev’s 1d Majorana chain, which offers a natural language for describing Wannierizable higher-order TSCs. A BdG system satisfying the Kitaev limit is termed a “Kitaev superconductor”, which generally admits a bulk energy gap and a symmetric description with maximally localized BdG Wannier functions.

Focusing on 2d class D systems with a spatial inversion symmetry, we identify four inequivalent minimal Kitaev superconductors (the Kitaev building blocks) as a complete set of basis for building general Kitaev superconductors. In particular, by stacking these Kitaev building blocks, we are able to systematically construct various Kitaev superconductors with intrinsic higher-order topology. Interestingly, some of the higher-order topological Kitaev superconductors share the same inversion eigenvalues at high-symmetry momenta with those of a trivial superconductor, which are thus beyond the detection of existing symmetry indicators in the literature. To overcome such difficulty of diagnosis, we propose a simple but powerful Majorana counting rule, arising naturally from our Kitaev construction, that correctly diagnoses the existence of higher-order topology for all Kitaev superconductors (including those beyond-indicator models).

To confirm our Majorana counting rule, we present two different stacking strategies with the Kitaev building blocks that have in principle exhausted all possible configurations for Kitaev superconductors. For each stacking strategy, we derive explicit “stacking recipes” based on our counting rule, which efficiently predict possible stacking configurations with higher-order topology. To demonstrate these ideas, we provide several minimal models for distinct stacking strategies and confirm their higher-order topological nature. The great success of the Majorana counting rule inspires us to conjecture a universal topological diagnosis for all Wannierizable superconductors. To demonstrate this conjecture, we discuss a realistic higher-order TSC model with fragile Wannier obstruction. Following the universal diagnosis, we decompose this model in terms of our Kitaev building blocks and explain the origin of its higher-order topology with our counting rule.

The introduction of the “Kitaev limit” as the funda-

mental building blocks for higher-order topological superconductors as well as the introduction of the new Majorana counting rule are the two important new concepts in our work. We show that these new concepts enable both the construction of higher-dimensional topological superconductors as well as the diagnosis for already-proposed higher-order topological superconductors, thus establishing our ideas as the foundation for the “Quantum Chemistry” of Topological Superconductors.

This paper is organized as follows. In Sec. II, we first present the main results of our work providing our definitions of higher-order topology, the Kitaev limit, and the Majorana counting rule. In Sec. III, we define the Kitaev building blocks and classify all Kitaev superconductors with the concept of 2d polarization. We then explicitly derive the Majorana counting rule as a necessary and sufficient condition for higher-order topology for Kitaev superconductors. In Sec. IV, we provide explicit constructions of Kitaev superconductors with higher-order topology to demonstrate our Majorana counting rule for different stacking strategies. The beyond-indicator models are presented and discussed in this section. In Sec. V, we conjecture a possible universal diagnosis for higher-order topology in all Wannierizable superconductors, as well as those with fragile Wannier obstructions. This conjecture is verified in Sec. VI for a realistic example that hosts both higher-order topology and fragile Wannier obstruction. The conclusion is presented in Sec. VII.

II. MAIN RESULTS

This section summarizes our main results in this work. We first provide a definition of symmetry-protected higher-order topology for 2d class D superconductors. We then define the Kitaev limit, a key concept in this work and a natural language for describing higher-order topological superconductors. Finally, we present a simple Majorana counting rule as a higher-order topological diagnosis for general Kitaev superconductors.

A. What is a Higher-order Topological Superconductor?

A 2d class D superconductor is defined to have symmetry-protected higher-order topology if

- (i) its bulk BdG spectrum is gapped;
- (ii) it has no 1d anomalous Majorana boundary modes;
- (iii) it has 0d Majorana zero modes exponentially localized on its symmetric boundary;
- (iv) while preserving the symmetry, the Majorana zero modes cannot be eliminated without closing the bulk gap.

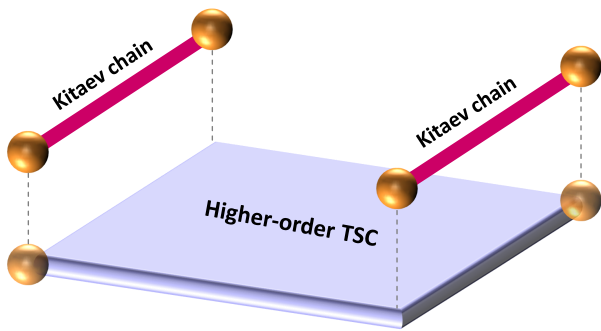


FIG. 1. A schematic of 2d inversion-protected higher-order TSC with a pair of corner-localized Majorana modes. To preserve the inversion symmetry, the Kitaev chains attached to the edge must come in pairs. Since a pair of Kitaev chains will necessarily add 4 Majorana zero modes to the edge, the corner Majorana physics cannot be essentially eliminated.

This definition is inspired by the phenomenological fact that a 2d higher-order TSC generally features gapped edge states and 0d boundary Majorana modes that are most likely localized around the corners. Notably, the presence of 0d boundary Majorana modes does not guarantee a bulk higher-order topology by itself. It is the necessary crystalline-symmetry protection that promotes such 0d boundary Majorana modes to a hallmark of non-trivial bulk topology.

The crucial role of symmetry protection can be understood as follows. Consider a 2d higher-order TSC with a (crystalline) symmetry \mathcal{G} on a symmetry-preserving open geometry. We then define $\mathcal{N}_{\mathcal{G}}$ as the number of 0d Majorana modes on the 1d edge “modulo” the symmetry \mathcal{G} . Namely, if two distinct boundary Majorana modes are related by any symmetry operation in $\mathcal{N}_{\mathcal{G}}$, they will be counted as the same Majorana mode in defining $\mathcal{N}_{\mathcal{G}}$. If $\mathcal{N}_{\mathcal{G}}$ is odd, it is obvious that the 0d Majorana modes cannot be eliminated by any \mathcal{G} -preserving edge perturbation (e.g. attaching 1d Kitaev chains in a \mathcal{G} -symmetric way). This robustness of 0d Majorana modes is exactly a manifestation of \mathcal{G} -protected higher-order bulk-boundary correspondence. This analysis also provides an alternative yet equivalent definition that *a 2d class D superconductor is \mathcal{G} -protected higher-order topological if and only if $\mathcal{N}_{\mathcal{G}}$ is odd.*

In this work, we focus on the BdG systems with 2d spatial inversion symmetry \mathcal{I} to demonstrate our general theory of higher-order TSCs. Practically, $\mathcal{N}_{\mathcal{I}}$, the number of Majorana zero modes modulo \mathcal{I} , can be simply counted on one x -edge and one y -edge, as well as the corner shared by the edges. Then by definition, an inversion-protected higher-order TSC is typically featured by two Majorana modes that are spatially separated at the opposite corners [30]. As a schematic example in Fig. 1, symmetrically coupling Kitaev chains to the boundary of an inversion-symmetric higher-order TSC can only shift the position of corner Majorana modes, but can never elim-

inate them. Therefore, this boundary configuration is stable against any boundary perturbations that preserve inversion symmetry, a hallmark of inversion-protected higher-order topology.

The higher-order TSCs that will be discussed in this work are Wannierizable, similar to recently proposed electronic insulators with fractional corner charges [25, 63–65]. Notice that the Wannierizability of corner-charged electron systems prevent them from having stable gapless bound states at the edges, since such bound state can always be removed by an applied smooth potential at the edge. In contrast, in-gap 0d Majorana modes on the boundary of a higher-order topological superconductor are robustly pinned at zero energy by the particle-hole symmetry. This crucial difference thus allows the existence of Wannierizable topological superconductors, which turn out to be most likely higher-order topological. This is one important motivation for us to consider Wannierizable higher-order topological BdG systems in this work.

B. Kitaev Limit for Superconductors

Higher-order topological superconductors are defined by the existence of anomalous unpaired Majorana modes at the boundaries. Following Kitaev [7], representing a BdG Hamiltonian in terms of Majorana fermions provides a natural representation to include the particle-hole symmetry. However, such Majorana representation introduces an additional constraint, which has no analog in the case of insulators, that Majorana fermions must appear in pairs on any so-called atomic site. For the purpose of superconductors, an “atomic site” \mathbf{R} is any position that we place a pair of Majorana fermions (or equivalently an electron and a hole) in the discretized BdG Hamiltonian. The on-site transformation between an electron operator $c_{\mathbf{R}}^{\dagger}$ and the corresponding pair of Majorana fermions $\alpha_{\mathbf{R}}$ and $\beta_{\mathbf{R}}$ is given by $c_{\mathbf{R}}^{\dagger} = (\alpha_{\mathbf{R}} - i\beta_{\mathbf{R}})/\sqrt{2}$.

A big advantage of the Majorana representation is that the electron-electron, hole-hole, and electron-hole couplings now become coupling or bondings among the Majorana operators. As shown in Fig. 2, when two Majorana fermions (the red and blue dots) are coupled with each other, we can pictorially connect them with a line to demonstrate the existence of a Majorana bond. In this work, we only consider the Majorana bonds that are local in space. Based on the Majorana representation, we define a special class of BdG systems:

- In the Majorana representation, a BdG system with periodic boundary conditions is in the “*Kitaev limit*”, if every Majorana fermion is attached to exactly one Majorana bond. Such BdG system is termed as a Kitaev superconductor.

The Kitaev limit is one of the key concepts in our work. It is physically motivated by the pioneering work

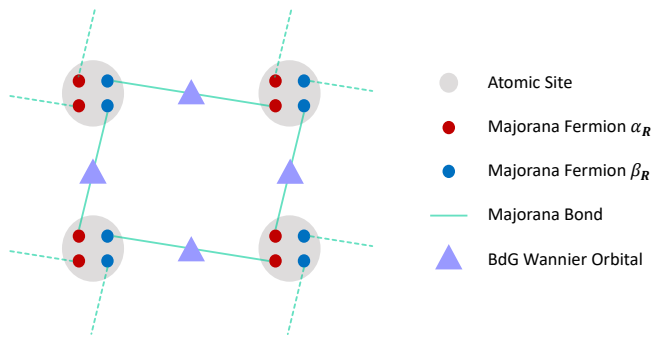


FIG. 2. An example of Kitaev limit with two pairs of Majorana fermions within each unit cell. Each Majorana fermion has exactly one Majorana bond attached. The maximally localized Wannier orbital sits at each bond center.

of Kitaev [7], in which he found a special limit of a 1d spinless p-wave superconductor model (often known as a Kitaev chain) that is exactly solvable. While Kitaev’s original idea aims at understanding the boundary physics in 1d class D TSCs, we generalize this concept to two and higher dimensions for any symmetry class [66]. We will see that the concept of Kitaev limit provides a natural framework to describe higher-order topological superconductors with 0d Majorana zero modes.

We emphasize that all Kitaev superconductors are featured by both a *bulk energy gap* and a description with *maximally localized BdG Wannier functions*. The bulk gap arise from the fact that every Majorana fermion is uniquely paired with another nearby Majorana fermion. The Majorana bond also leads to an exponentially localized Wannier function sitting at the bond center. For a Kitaev superconductor with bonds connecting only on-site or nearest-neighboring Majorana fermions, the range of the Wannier function is restricted within one unit cell. Adding any additional Majorana bonds to this Kitaev superconductor will only further delocalize the spatial profile of the Wannier function. This is why the Wannier functions of a Kitaev superconductor are maximally localized. Since the Majorana representation and the Wannier representation with maximally localized Wannier orbitals are essentially the two sides of the same coin, they will be used interchangeably in this work.

A schematic example of a 2d Kitaev superconductor is shown in Fig. 2. Within one unit cell, we have considered two atomic sites (the gray disks) that coincide with each other [67]. Each atomic site hosts a pair of Majorana fermions $\alpha_{\mathbf{R}}$ (the red dot) and $\beta_{\mathbf{R}}$ (the blue dot). In particular, every Majorana fermion is only connected to one distinct Majorana fermions through a intersite Majorana bond (the green line), which clearly satisfies the definition of Kitaev limit. For demonstration, we also plot the maximally localized BdG Wannier orbitals (the purple triangles) sitting at the bond center.

Our definition of the Kitaev limit relies on physical Majorana degrees of freedom and thus distinguishes a

superconducting BdG system from a particle-hole symmetric electron system with no superconductivity. This fact is crucial for discussing a topological classification for superconductors.

C. Condition of Higher-order Topology for Kitaev Superconductors

If an inversion-symmetric Kitaev superconductor has $n_i^{(A)}$ atomic sites and $n_i^{(W)}$ Wannier orbitals at maximal Wyckoff position \mathbf{q}_{1i} for $i \in \{a, b, c, d\}$, it has inversion-protected higher-order topology *if and only if*

$$\Delta_{b,c,d} \equiv 1 \pmod{2}. \quad (1)$$

where we have defined a set of Majorana counting numbers as

$$\Delta_i = n_i^{(W)} - n_i^{(A)}. \quad (2)$$

This simple counting of bulk atomic sites and Wannier orbitals provide a necessary and sufficient condition for a general Kitaev superconductor to be higher-order topological, which is thus dubbed the “Majorana counting rule”.

For 2d inversion-symmetric systems, we have defined the maximal Wyckoff positions as the real-space positions invariant under \mathcal{I} operation, up to lattice translations. Within one unit cell, we label the maximal Wyckoff positions as

$$\begin{aligned} \mathbf{q}_{1a} &= (0, 0), & \mathbf{q}_{1b} &= \left(\frac{1}{2}, 0\right), \\ \mathbf{q}_{1c} &= \left(0, \frac{1}{2}\right), & \mathbf{q}_{1d} &= \left(\frac{1}{2}, \frac{1}{2}\right), \end{aligned} \quad (3)$$

where the lattice constants are set to be $\mathbf{a}_x = \mathbf{a}_y = 1$ for simplicity.

Physically, the position information of atomic sites determines how crystalline symmetries are implemented in a BdG system, which provides necessary symmetry constraint for choosing a symmetric open boundary. Therefore, it is the countings of both atomic sites and Wannier orbitals that together determine the boundary Majorana information on a symmetric Kitaev superconductor.

We will explicitly derive the Majorana counting rule in the coming Sec. III D. The concept of Kitaev limit and the Majorana counting rule are the most important results in this work.

III. CLASSIFICATION OF KITAEV SUPERCONDUCTORS AND MAJORANA COUNTING

In this section, we will elaborate on our main results summarized in the previous section by systematically classifying 2d Kitaev superconductors and explicitly deriving the Majorana counting rule as a powerful diagnosis for higher-order topology.

A. Kitaev Building Blocks

The key to classify all these Kitaev superconductors for a specific symmetry class is to identify a set of minimal/simplest symmetry-allowed Kitaev superconductors as a complete basis, based on which one can construct more complicated situations. This set of minimal Kitaev superconductors are termed “Kitaev building blocks”. For a symmetry group G , the d -dimensional Kitaev building blocks are defined as all d -dimensional Kitaev superconductors that (i) preserve all symmetries in G ; (ii) can NOT be decomposed into a superposition of any other G -preserving d -dimensional Kitaev superconductors.

For 2d class D Kitaev superconductors with inversion symmetry, there exist four distinct Kitaev building blocks κ_i with $i \in \{a, b, c, d\}$, which are constructed by placing one atomic site at \mathbf{q}_{1a} and one *maximally localized* BdG Wannier orbital at a maximal Wyckoff position \mathbf{q}_{1i} in the Wannier representation.

While a Wannier orbital could be even (s-like) or odd (p-like) under inversion operation, the specific orbital type is irrelevant for our most discussions. In Fig. 3 (a) - (d), we schematically plot those four Kitaev building blocks $\kappa_{a,b,c,d}$. As before, we use the gray disk at \mathbf{q}_{1a} to denote the atomic sites and the colored dots to denote the maximally localized Wannier orbitals. Map the Wannier representation back to the Majorana representation, we arrive at Fig. 3 (e) - (h), which demonstrate the Majorana bonding configurations for the Kitaev building blocks.

In principle, one can always place a Wannier orbital on some non-maximal Wyckoff position \mathbf{q}_α that is not invariant under inversion operation \mathcal{I} . Then we are required to place another Wannier orbital at a different but inversion-related Wyckoff position $\mathcal{I}\mathbf{q}_\alpha$ just to preserve the inversion symmetry. On the other hand, we can always simultaneously move the Wannier orbital at \mathbf{q}_α and the other one at $\mathcal{I}\mathbf{q}_\alpha$ to any maximal Wyckoff position in an adiabatic and symmetric way. Therefore, putting Wannier orbitals on non-maximal Wyckoff positions is always equivalent to a double-stacking of some Kitaev building blocks κ_i . This is why the four Kitaev building blocks in Fig. 3 form a complete basis set for general Kitaev superconductors.

B. Polarization and Topological Classification for Kitaev Superconductors

To further characterize the topological properties of Kitaev building blocks, we define a 2d polarization $\mathcal{P} = (P_x, P_y)$ for Kitaev superconductors as the net relative displacement vector between the atomic sites and the Wannier orbitals, where $P_{x,y}$ are defined modulo the lattice constants. By definition, the polarization \mathcal{P}_{κ_i} for a Kitaev building block κ_i is exactly the Wyckoff position

of its Wannier orbital,

$$\mathcal{P}_{\kappa_i} = \mathbf{q}_{1i}. \quad (4)$$

It should be emphasized that our definition for the polarization \mathcal{P} of Kitaev superconductors is *purely geometric*. In particular, \mathcal{P} should NOT be confused with the physical charge polarization for insulators [68], which is only well-defined in the presence of charge $U(1)$ symmetry. Here we use the term “polarization” for \mathcal{P} just to follow the convention in electron systems.

It is straightforward to see that inversion symmetry requires both components of polarization vector $P_{x,y}$ to be quantized to either 0 or $1/2$ modulo 1. In addition, we find the quantized value of \mathcal{P} is directly linked with weak topological phenomena. When $P_{x(y)} = 1/2$, the Kitaev superconductor displays weak topology [69], with its edge normal to the $x(y)$ -direction hosting a non-degenerate edge Majorana flat band.

A pictorial understanding of the weak topology for the Kitaev building blocks is clearly explained in Fig. 3 (e) - (h). Take the building block κ_d with $\mathcal{P} = (1/2, 1/2)$ as an example. As shown in Fig. 3 (h), κ_d on an open geometry clearly hosts unpaired Majorana zero modes [colored circles in Fig. 3 (h)] in both x and y edges. If we calculate the edge spectrum for κ_d , the unpaired Majorana modes will form a single flat band at exactly zero energy for both x and y edges, a hallmark for 2d weak TSCs. Similarly shown in Fig. 3 (b) and (c), κ_b and κ_c also host non-degenerate edge Majorana flat bands on their x and y edges, respectively. Their \mathcal{P} values agree with the existence of weak topology. Since all Kitaev superconductors can be constructed with the Kitaev building blocks, it is clear that this bulk-boundary correspondence between \mathcal{P} and edge Majorana bands should generally hold.

For each building block with open boundary conditions, it is straightforward to count the dangling Majorana zero modes on the boundary. In Fig. 3 (e) - (h), we use N_x and N_y to respectively denote the numbers of dangling Majorana modes on each x and y edge. We explicitly show how $N_{x,y}$ scale with $L_{x,y}$, which are the numbers of unit cells along x and y directions. Notably, (N_x, N_y) will provide an important input for deriving the Majorana counting rule in Sec. III D.

In principle, one can go beyond the Kitaev limit and deform a completely flat edge Majorana band into a dispersing one, as shown in Fig. 4. Such dispersing Majorana edge band is also anomalous and cannot be realized in any 1d bulk BdG system. This is because particle-hole symmetry will require the edge Majorana band to cross zero energy at $k_{\text{edge}} = 0, \pi$, manifesting its Majorana nature.

With the bulk-boundary correspondence of \mathcal{P} , we now classify all 2d Kitaev superconductors into three topologically inequivalent classes: (i) trivial Kitaev superconductors with no weak or higher-order topology; (ii) weak TSCs with $\mathcal{P} \neq 0$; (iii) higher-order TSCs with $\mathcal{P} = 0$.

Even beyond the Kitaev limit, we still expect that this topological classification should generally hold for any 2d

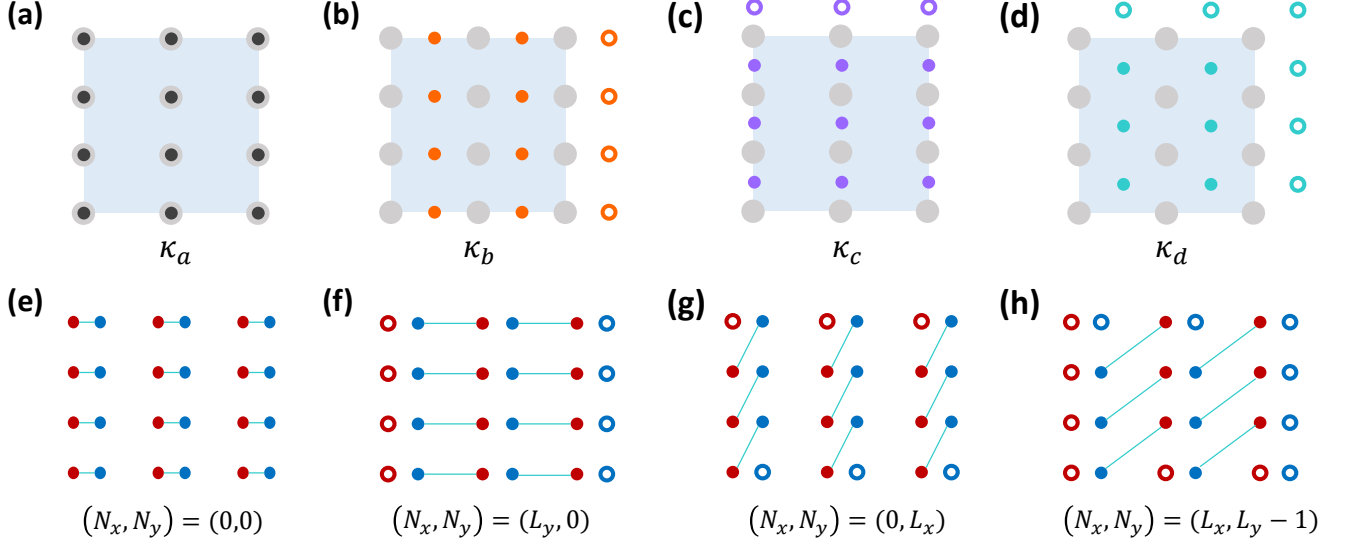


FIG. 3. The Wannier representations and the Majorana representations for each Kitaev building block are shown in (a) - (d) and (e) - (h), respectively. The dangling Wannier orbitals and Majorana zero modes are shown in colored circles. (N_x, N_y) shows the numbers of dangling Majorana zero modes for one x edge and one y edge, respectively.

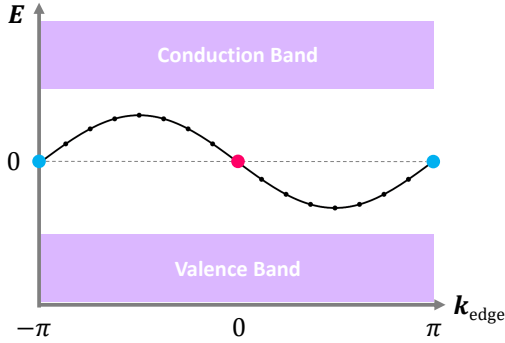


FIG. 4. A schematic for a dispersing edge Majorana band in a weak TSC. This edge band is anomalous and is enforced to cross zero energy at high-symmetry momenta (colored dots) in the edge Brillouin zone.

Wannierizable superconductors.

C. Atomic Site, Stacking, and Open Boundary Conditions

Now let us elaborate on another key ingredient for understanding the higher-order topology in Kitaev superconductors, which is the role of atomic sites in defining an inversion-symmetric open boundary. With the Kitaev building blocks as a complete set of basis, we will show that the choice of symmetric open boundary is closely related to how we “stack” the Kitaev building blocks.

In principle, there are two distinct stacking strategies with the Kitaev building blocks to generate all possible

Kitaev superconductors:

- *Face-to-face stacking*: The atomic sites of all stacked building block coincide with each other in real space at \mathbf{q}_{1a} .
- *Displaced stacking*: The atomic sites of some stacked building blocks are different from \mathbf{q}_{1a} .

As a reference point, we always assume the existence of at least one building block, whose atomic site coincides with the origin \mathbf{q}_{1a} . For the displaced stacking, when we place the atomic site of a Kitaev building block κ_i at some general/maximal Wyckoff position \mathbf{q} , we also put its corresponding Wannier orbital at $\mathbf{q} + \mathbf{q}_{1j}$ in order to make the building block well-defined.

After the face-to-face stacking, the composite system has no sublattice degree of freedom. Since the inversion center is always set at the origin \mathbf{q}_{1a} in our convention, any rectangular open geometry with an odd-integer number of unit cells along x and y directions would preserve the inversion symmetry.

For the displaced stacking, however, the collection of atomic sites within one single unit cell are not invariant under its inversion center as a whole. Therefore, in an open geometry with an integer number of unit cells, we will inevitably eliminate some atomic sites on the boundary to preserve the global inversion. For illustration, we plot in Fig. 5 four inequivalent displaced stacking configurations. For an open geometry with $L_x \times L_y$ unit cells ($L_{x,y} \in \text{odd}$), if we place one atomic site at \mathbf{q}_{1a} and another at \mathbf{q}_{1b} (\mathbf{q}_{1c}), the number of atomic sites being disregarded (shown in red circle) is exactly L_y (L_x), as shown in Fig. 5 (a) and (b). If we place one atomic site

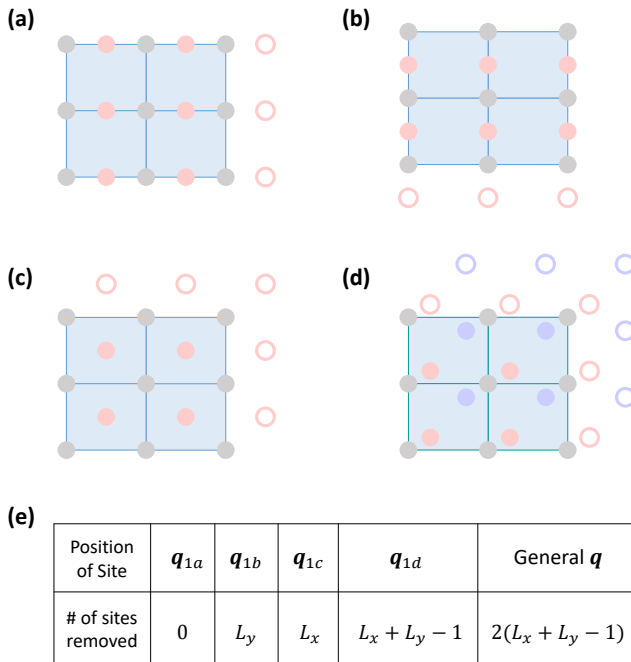


FIG. 5. The solid dots form inversion-symmetric open lattice geometries for atomic site configurations in (a) - (d). Boundary atomic sites that need to be eliminated to preserve inversion symmetry are shown in colored circles. In (e), we list the number of atomic sites that need to be removed for an open geometry with $L_x \times L_y$ unit cells if we assign an atomic site to a specific Wyckoff position.

at \mathbf{q}_{1a} and another at \mathbf{q}_{1d} , the number of sites being ignored is actually $L_x + L_y - 1$, with this extra -1 coming from the corner atomic site shared by the x and y edges, as shown in Fig. 5 (c). On the other hand, if an atomic site (red dot) is placed at a non-maximal Wyckoff position \mathbf{q} , there must be another atomic site (purple dot) at the inversion-related position $\mathcal{I}\mathbf{q}$ to preserve the inversion symmetry, as shown in Fig. 5 (d). In this case, the number of removed atomic sites on the boundary is $2(L_x + L_y - 1)$. To summarize, we have listed the results in Fig. 5 (e).

D. The Majorana Counting Rule: A Derivation

Now we are ready to derive the bulk Majorana counting rule for Kitaev superconductors.

As shown in Fig. 3, we first notice that the number of dangling Majorana modes for each Kitaev building blocks is exactly half the number of dangling Wannier orbitals in its Wannier representation. This is simply because the Wannier orbitals in Fig. 3 are only shown for the occupied states, while their particle-hole partners for the unoccupied states exactly sit at the same location. Similar to a Kitaev chain, such particle-hole pair of Wannier orbitals on the boundary essentially originate from a non-

local superposition of one α -type Majorana fermion and one β -type Majorana fermion. This completes the mapping between the Majorana representation and the Wannier representation for a general Kitaev limit with open boundary conditions.

Recall that in Fig. 3, we also list (N_x, N_y) for each building block with L_x by L_y unit cells. So one might naively expect that, $\mathcal{N}_{\mathcal{I}}(\kappa_i)$, the number of boundary Majorana modes modulo \mathcal{I} for a building block κ_i , is simply $N_x + N_y$. However, we will then have missed a crucial fact that some boundary atomic sites must be removed along with their Wannier orbitals to preserve the inversion symmetry, as we have discussed in Sec. III C.

To implement a correct counting of boundary Majorana modes, we consider a general Kitaev limit with $n_i^{(A)}$ atomic sites and $n_i^{(W)}$ Wannier orbitals at maximal Wyckoff position \mathbf{q}_{1i} . On an open geometry with complete $L_x \times L_y$ unit cells, we have $\mathcal{N}_{\mathcal{I}}^{(0)} = L_y n_b^{(W)} + L_x n_c^{(W)} + (L_x + L_y - 1)n_d^{(W)}$ Majorana modes dangling on the boundary. On the other hand, following Fig. 5 (e), we also need to remove $\mathcal{N}_{\mathcal{I}}^{(1)} = L_y n_b^{(A)} + L_x n_c^{(A)} + (L_x + L_y - 1)n_d^{(A)}$ numbers of atomic sites along with their Wannier orbitals (or equivalently boundary Majorana modes). All these countings together lead to

$$\mathcal{N}_{\mathcal{I}} = L_x(\Delta_c + \Delta_d) + L_y(\Delta_b + \Delta_d) - \Delta_d, \quad (5)$$

where we have defined the Majorana counting number $\Delta_i = n_b^{(W)} - n_b^{(A)}$. Since we only care about the oddness of $\mathcal{N}_{\mathcal{I}}$, we will not count any contributions from both atomic sites and Wannier orbitals at a non-maximal Wyckoff position, which only contribute evenly to $\mathcal{N}_{\mathcal{I}}$.

On the other hand, we hope to rule out the possibility of weak TSCs by imposing a polarization constraint $\mathcal{P} = 0$. It is then straightforward to show that a vanishing \mathcal{P} is equivalent to

$$\Delta_b + \Delta_d \equiv \Delta_c + \Delta_d \equiv 0 \pmod{2}. \quad (6)$$

Together with Eq. 5, we find that the condition for hosting higher-order topology with an odd $\mathcal{N}_{\mathcal{B}\mathcal{I}}$ is only possible when $\Delta_{b,c,d}$ are all odd. This is exactly the Majorana counting rule that we have stated in Sec. II C. Remarkably, this simple counting rule only relies on the position information of atomic sites and Wannier orbitals.

In the following section, we will construct explicit examples to demonstrate both the stacking-based construction of Kitaev superconductors with higher-order topology and how they can be correctly diagnosed via the Majorana counting rule.

IV. BUILDING-BLOCK CONSTRUCTION OF HIGHER-ORDER TSCS

In this section, we construct explicit examples of Kitaev superconductors with higher-order topology following different stacking strategies. In particular, we will

propose several stacking recipes as a guidance for constructing higher-order TSC phases. Some of the examples are beyond the detection of the existing symmetry indicators.

A. Face-to-face Stacking

Let us first focus on the face-to-face stacking strategy. Starting from the Majorana counting rule, we first derive a simple stacking recipe that necessarily leads to higher-order topology. We will then construct a minimal face-to-face stacking model with higher-order topology that demonstrate both the stacking recipe and the counting rule.

1. Recipe of Face-to-face Stacking

For face-to-face stacking of the Kitaev building blocks, by definition, all the atomic sites sit at the unit-cell origin \mathbf{q}_{1a} . Therefore, if we stack n_i copies of building block κ_i with $i = a, b, c, d$, the counting numbers are given by

$$\begin{aligned}\Delta_a &= -(n_b + n_c + n_d), \quad \Delta_b = n_b, \\ \Delta_c &= n_c, \quad \Delta_d = n_d.\end{aligned}\quad (7)$$

According to the Majorana counting rule, we immediately arrive at the following stacking recipe for higher-order TSC:

- **Stacking Recipe #1:** Face-to-face stacking n_i copies of building block κ_i ($i = a, b, c, d$) will lead to higher-order topology *if and only if* $n_{b,c,d} \in \text{odd}$.

According to this recipe, the minimal face-to-face stacking model that hosts higher-order topology is to choose $n_b = n_c = n_d = 1$. In the following, we will construct such minimal tight-binding model and explicitly demonstrate the existence of corner-localized Majorana zero modes.

2. A Minimal Face-to-face Stacking Model with Higher-order Topology

We consider three electron orbitals labeled by an orbital index $l = b, c, d$ at Wyckoff position \mathbf{q}_{1a} , as well

as the corresponding hole partners. The electron annihilation and creation operators can be written as a linear superposition of Majorana operators $\alpha_{\mathbf{R},l}$ and $\beta_{\mathbf{R},l}$ as

$$c_{\mathbf{R},l} = \frac{\alpha_{\mathbf{R},l} + i\beta_{\mathbf{R},l}}{\sqrt{2}}, \quad c_{\mathbf{R},l}^\dagger = \frac{\alpha_{\mathbf{R},l} - i\beta_{\mathbf{R},l}}{\sqrt{2}}. \quad (8)$$

A schematic plot of the lattice configuration in the Majorana representation is shown in Fig. 6 (a), where the red dots and the blue dots denote α -type and β -type Majorana degrees of freedom, respectively.

To realize the face-to-face stacking, we introduce the following inter-unit-cell Majorana bonds shown in Fig. 6 (a):

- (i) the red bond t_1 connects $\alpha_{\mathbf{R},b}$ and $\beta_{\mathbf{R}+\mathbf{a}_x,b}$, which realizes a copy of κ_b with $\mathcal{P} = (\frac{1}{2}, 0)$;
- (ii) the purple bond t_2 connects $\alpha_{\mathbf{R},c}$ and $\beta_{\mathbf{R}+\mathbf{a}_y,c}$, which realizes a copy of κ_c with $\mathcal{P} = (0, \frac{1}{2})$;
- (iii) the green bond t_3 connects $\alpha_{\mathbf{R},d}$ and $\beta_{\mathbf{R}+\mathbf{a}_x+\mathbf{a}_y,d}$, which realizes a copy of κ_d with $\mathcal{P} = (\frac{1}{2}, \frac{1}{2})$.

As a demonstration, the configuration of BdG Wannier orbitals is schematically plotted in Fig. 6 (c), where the color of each Wannier orbital matches with that of its corresponding Majorana bond.

While the colored Majorana bonds necessarily gap out the bulk states, there are still some unwanted dangling Majorana modes (or equivalently dangling Wannier orbitals) on the edge, as shown by the open circles in Fig. 6 (a) and (c). To further remove these in-gap edge degree of freedom, we introduce additional *weak* Majorana bonds among different species of Majorana modes within one unit cell, as shown by the black dashed lines. Therefore, in terms of Majorana operators, the Hamiltonian consists of h_{sb} describing the colored strong bonds and h_{wb} for the dashed weak bonds. In the Majorana representation, we have

$$\begin{aligned}h_{sb} &= i \sum_{\mathbf{R}} [t_1 \alpha_{\mathbf{R},b} \beta_{\mathbf{R}+\mathbf{a}_x,b} + t_2 \alpha_{\mathbf{R},c} \beta_{\mathbf{R}+\mathbf{a}_y,c} + t_3 \alpha_{\mathbf{R},d} \beta_{\mathbf{R}+\mathbf{a}_x+\mathbf{a}_y,d}], \\ h_{wb} &= \sum_{\mathbf{R}} [iu_{12}(\alpha_{\mathbf{R},b} \alpha_{\mathbf{R},c} + \beta_{\mathbf{R},b} \beta_{\mathbf{R},c}) + iu_{23}(\alpha_{\mathbf{R},c} \alpha_{\mathbf{R},d} + \beta_{\mathbf{R},c} \beta_{\mathbf{R},d}) + iv_{12}(\alpha_{\mathbf{R},b} \beta_{\mathbf{R},c} + \alpha_{\mathbf{R},c} \beta_{\mathbf{R},b}) \\ &\quad + iv_{23}(\alpha_{\mathbf{R},c} \beta_{\mathbf{R},d} + \alpha_{\mathbf{R},d} \beta_{\mathbf{R},c})].\end{aligned}\quad (9)$$

In the momentum space, we consider the following BdG

basis

$$\Psi(\mathbf{k}) = (c_{\mathbf{k},b}, c_{\mathbf{k},c}, c_{\mathbf{k},d}, c_{-\mathbf{k},b}^\dagger, c_{-\mathbf{k},c}^\dagger, c_{-\mathbf{k},d}^\dagger)^T, \quad (10)$$

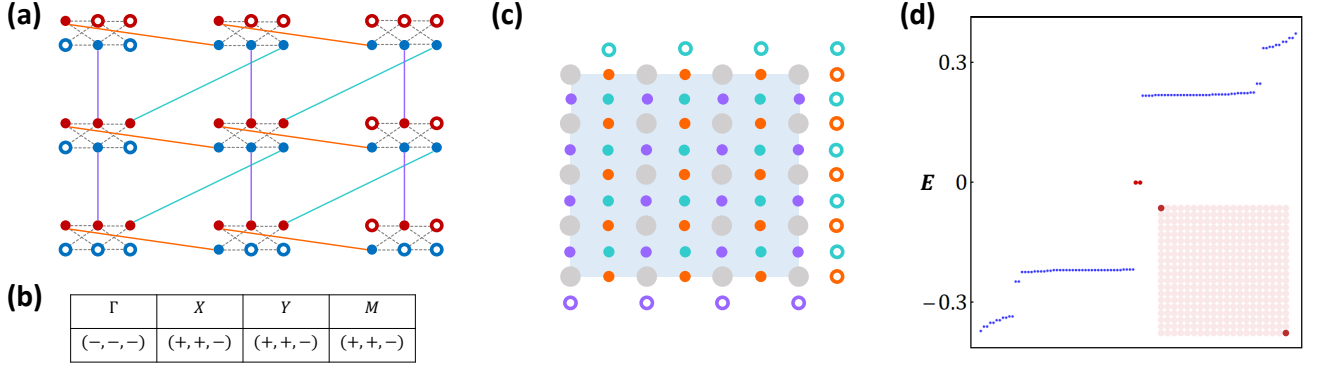


FIG. 6. Our minimal model for a nontrivial face-to-face stacking in the Majorana representation is shown (a). The red and blue dots denote α and β Majorana fermions, while the colored circles in (a) denote unpaired boundary Majorana fermions for h_{sb} . In particular, the colored solid (black dashed) lines denote the strong Majorana bonds in h_{sb} (weak Majorana bonds in h_{wb}). The parity data for each high-symmetry momentum is shown in (b). We plot in (c) the distribution of BdG Wannier orbitals, with the large grey dots for the atomic sites and the small colored dots (or circles) for the Wannier orbitals. (d) shows the energy spectrum of $H_1(\mathbf{k})$ in an open geometry. There exists a pair of Majorana zero-energy modes (highlighted in red) that are localized on the top-left and bottom-right corners, as shown in the inset of (d).

and the above Hamiltonians become

$$H_1(\mathbf{k}) = \begin{pmatrix} t_1 \cos k_x & iu_{12} + v_{12} & 0 & it_1 \sin k_x & 0 & 0 \\ -iu_{12} + v_{12} & t_2 \cos k_y & iu_{23} + v_{23} & 0 & it_2 \sin k_y & 0 \\ 0 & -iu_{23} + v_{23} & t_3 \cos(k_x + k_y) & 0 & 0 & it_3 \sin(k_x + k_y) \\ -it_1 \sin k_x & 0 & 0 & -t_1 \cos k_x & iu_{12} - v_{12} & 0 \\ 0 & -it_2 \sin k_y & 0 & -iu_{12} - v_{12} & -t_2 \cos k_y & iu_{23} + v_{23} \\ 0 & 0 & -it_3 \sin(k_x + k_y) & 0 & -iu_{23} + v_{23} & -t_3 \cos(k_x + k_y) \end{pmatrix} \quad (11)$$

The inversion operator for the bulk Hamiltonian $H_1(\mathbf{k})$ is given by $\mathcal{I} = \tau_z \otimes \mathbb{1}_3$. Here τ_z is a Pauli matrix for the particle-hole index and $\mathbb{1}_3$ is a 3×3 identity matrix characterizing the orbital index l . For our choice of parameters, it is easy to check that the parity data for the occupied bands at each high-symmetry momenta is given by Fig. 6 (b). Notably, such parity data directly implies a “double band inversion” at Γ point [51] and agrees with a prediction of higher-order TSC from existing symmetry indicators [57, 59–61].

To confirm $H_1(\mathbf{k})$ as a higher-order TSC, we calculate its energy spectrum on a square lattice with open boundary conditions in both x and y directions. As shown in Fig. 6 (d) and its inset, we indeed find a pair of corner-localized Majorana zero modes, which unambiguously demonstrate the inversion-protected higher-order topology in our system. We note that the corner Majorana modes in H_f has vanishing localization length, which is similar to the Kitaev limit of a 1d Majorana chain. This numerical result agrees with our Majorana counting rule and the stacking recipe #1.

In fact, we do expect that symmetry-eigenvalue-based diagnosis can determine the higher-order topology for all our face-to-face stacking models. This is related to the

fact that face-to-face stacking models are defined to have momentum-independent representation for the inversion symmetry, as will be discussed in details in Sec. IV C 2.

B. Displaced Stacking with the Same Building Blocks

To go beyond the face-to-face stacking, we now turn to a more general situation where the building blocks are stacked in a displaced way. Specifically, the atomic sites of the building blocks do NOT have to coincide at \mathbf{q}_{1a} . This stacking strategy inspires us to define a displacement vector $\mathbf{d} = (d_x, d_y)$ to characterize the displacement between the atomic site and the origin \mathbf{q}_{1a} . Since only the atomic sites and Wannier orbitals sitting at maximal Wyckoff positions can contribute to the higher-order topology, the components of \mathbf{d} must be half-integer-valued with respect to the lattice constant with $d_{x,y} \in \{0, \frac{1}{2}\}$. From now on, we will denote that a building block is sitting at a Wyckoff position \mathbf{q} if its atomic site coincides with \mathbf{q} .

Let us first start with the displaced stacking construc-

tion with *only* one kind of building block, i.e. n_i copies of building block κ_i ($i = b, c, d$). To avoid Majorana edge band, we first require $n_i \in$ even to trivialize bulk polarization \mathcal{P} . In addition, we will ignore the case where an even number of building blocks of the same kind share the same atomic site, because such stacked system is always topologically trivial. As a result, it is sufficient to consider a simple double-stacking model with $n_i = 2$, where one building block κ_i sits at \mathbf{q}_{1j_1} and another building block κ_i sits at \mathbf{q}_{1j_2} for $j_1 \neq j_2 \in \{a, b, c, d\}$. Such double-stacking model is uniquely characterized by a *relative* displacement vector $\delta\mathbf{d}^{(i)} = \mathbf{q}_{1j_2} - \mathbf{q}_{1j_1}$, where the superscript i labels the type of building block.

For the double-stacking models, we have identified a necessary and sufficient condition for the presence of higher-order topology, which can be easily tested.

- **Stacking Recipe #2:** A double-stacking system with building block κ_i is higher-order topological *if and only if* the relative displacement vector $\delta\mathbf{d}^{(i)} \notin \{\mathbf{q}_{1a}, \mathbf{q}_{1i}\}$ for $i \in \{b, c, d\}$.

For example, a topologically trivial example can be constructed by placing one κ_b at \mathbf{q}_{1a} and another κ_b at \mathbf{q}_{1b} such that $\delta\mathbf{d}^{(b)} = \mathbf{q}_{1b}$. This can be understood from the Majorana counting rule, since we now have an equal number of atomic sites and Wannier orbitals for all maximal Wyckoff positions and consequently all Majorana counting numbers are zero.

However, if we move the κ_b at \mathbf{q}_{1b} to \mathbf{q}_{1c} , the system is then expected to be higher-order topological following the recipe, since $\delta\mathbf{d}^{(b)} = \mathbf{q}_{1c}$. From the counting perspective, we have one atomic site (Wannier orbital) at \mathbf{q}_{1a} and \mathbf{q}_{1c} (\mathbf{q}_{1b} and \mathbf{q}_{1d}), respectively, which directly indicates nontrivial counting numbers

$$\Delta_a = -\Delta_b = \Delta_c = -\Delta_d = -1 \quad (12)$$

In the remaining part of this subsection, we will check this prediction by constructing a corresponding minimal double-stacking model and explicitly demonstrating the existence of corner-localized Majorana zero modes.

1. A Minimal Double-Stacking Model with Higher-order Topology

The minimal double-stacking model with a relative displacement vector $\delta\mathbf{d}^{(b)} = \mathbf{q}_{1c}$ is schematically shown in Fig. 7 (a), where red and blue dots denote α -type and β -type Majorana operators. The lattice constants \mathbf{a}_x and \mathbf{a}_y are also shown in Fig. 7 (a). For our purpose, we include two pairs of Majorana modes within one unit cell, with one pair at $\mathbf{r}_A = \mathbf{q}_{1a} = (0, 0)$ with a sublattice index A and another pair at $\mathbf{r}_B = \mathbf{q}_{1c} = (0, \frac{1}{2})$ with an index B . The Majorana operators are related to the electron creation and annihilation operators as

$$c_{\mathbf{R},l} = \frac{\alpha_{\mathbf{R},l} + i\beta_{\mathbf{R},l}}{\sqrt{2}}, \quad c_{\mathbf{R},l}^\dagger = \frac{\alpha_{\mathbf{R},l} - i\beta_{\mathbf{R},l}}{\sqrt{2}}, \quad (13)$$

where $l = A, B$ is the sublattice index and \mathbf{R} is the lattice vector that defines the unit cell.

Three types of Majorana bonds are considered in this minimal model. As shown in Fig. 7 (a),

- (i) the green bond t connects $\beta_{\mathbf{R},l}$ and $\alpha_{\mathbf{R}+\mathbf{a}_x,l}$, which realizes a copy of κ_b for individual sublattice if they are the strongest bonds;
- (ii) the dashed orange bond m_α connects $\alpha_{\mathbf{R},B}$ and $\alpha_{\mathbf{R}+\mathbf{a}_y,A}$;
- (iii) the solid orange bond m_β connects $\beta_{\mathbf{R},A}$ and $\beta_{\mathbf{R},B}$.

Then the model Hamiltonian in the Majorana representation is given by

$$H_2(\mathbf{k}) = it\beta_{\mathbf{R},l}\alpha_{\mathbf{R}+\mathbf{a}_x,l} + im_\alpha\alpha_{\mathbf{R},B}\alpha_{\mathbf{R}+\mathbf{a}_y,A} + im_\beta\beta_{\mathbf{R}+\mathbf{a}_y,B}\beta_{\mathbf{R},A}. \quad (14)$$

The inversion operation will switch between α and β as

$$\mathcal{I} \begin{pmatrix} \alpha_{\mathbf{R},l} \\ \beta_{\mathbf{R},l} \end{pmatrix} = \begin{pmatrix} 0 & -1 \\ 1 & 0 \end{pmatrix} \begin{pmatrix} \alpha_{\mathbf{R}',l} \\ \beta_{\mathbf{R}',l} \end{pmatrix}, \quad (15)$$

where \mathbf{R} and \mathbf{R}' are related by inversion symmetry. It is easy to check that inversion symmetry will enforce $m_\alpha = m_\beta = m$.

Back to the fermion basis, we consider the Fourier transformation

$$c_{\mathbf{R},l} = \sum_{\mathbf{k}} e^{i\mathbf{k}\cdot(\mathbf{R}+\mathbf{r}_l)} c_{\mathbf{k},l}, \quad (16)$$

and the momentum-space Hamiltonian is

$$H_2(\mathbf{k}) = \begin{pmatrix} -t \cos k_x & -im \cos \frac{k_y}{2} & it \sin k_x & m \sin \frac{k_y}{2} \\ im \cos \frac{k_y}{2} & -t \cos k_x & m \sin \frac{k_y}{2} & it \sin k_x \\ -it \sin k_x & m \sin \frac{k_y}{2} & t \cos k_x & -im \cos \frac{k_y}{2} \\ m \sin \frac{k_y}{2} & -it \sin k_x & im \cos \frac{k_y}{2} & t \cos k_x \end{pmatrix}. \quad (17)$$

in the Nambu basis

$$\Psi(\mathbf{k}) = (c_{\mathbf{k},A}, c_{\mathbf{k},B}, c_{-\mathbf{k},A}^\dagger, c_{-\mathbf{k},B}^\dagger)^T. \quad (18)$$

We note that $H_x^{(d)}(\mathbf{k})$ can be diagonalized analytically with eigen-energy as

$$E = \pm \sqrt{m^2 + t^2 \pm 2mt \cos \frac{k_y}{2}}. \quad (19)$$

Therefore, there exists a topological phase transition (bulk gap closing) at $|t| = |m|$ that separate two distinct phases.

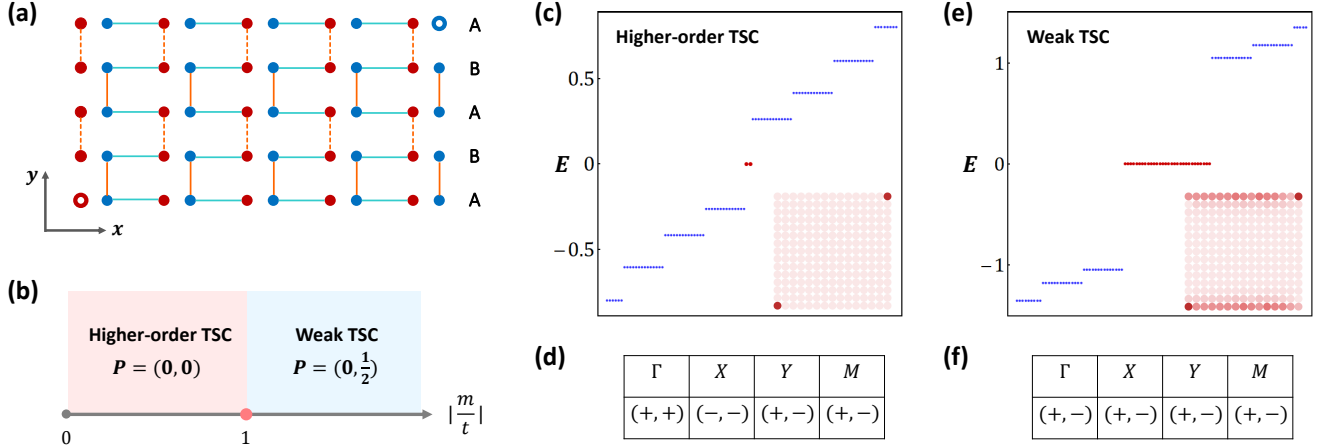


FIG. 7. The Majorana representation of the minimal double-stacking model $H_2(\mathbf{k})$ is shown in (a). The topological phase diagram of H_2 as a function of $|m/t|$ is shown in (b). We plot the energy spectrum for the higher-order TSC phase on an open geometry in (c) and list its parity data in (d). The energy spectrum and the parity data for the weak TSC phase with $\mathcal{P} = (0, \frac{1}{2})$ are shown in (e) and (f), respectively.

2. $H_2(\mathbf{k})$ with $|t| > |m|$: A Higher-order TSC

When $|t| > |m|$, we consider the Kitaev limit by setting $|m| \rightarrow 0$. Then the BdG Wannier orbitals of the double-stacking model are exactly localized at the center of the green Majorana bonds. Therefore, the system is equivalent to a stacking of one κ_b at \mathbf{q}_{1a} and another κ_b at \mathbf{q}_{1c} , which is featured by a relative displacement vector $\delta\mathbf{d}^{(b)} = \mathbf{q}_{1c}$. According to our stacking recipe #2, this phase is diagnosed to be a higher-order TSC.

To confirm its higher-order nature, we numerically calculate the energy spectrum of this double-stacking model with $t = 1.2$ and $m = 1$ on an open geometry. To preserve the inversion symmetry, it is crucial to choose only the atomic sites with a sublattice index $l = A$ as the edge termination for both the upper and the lower y -edges, similar to the lattice geometry in Fig. 7 (a). Just as we expect, the energy spectrum in Fig. 7 (c) hosts a pair of Majorana modes exactly at zero energy. In the inset of Fig. 7 (c), we further plot the wavefunction distribution in the real space for both Majorana modes. Sitting in the opposite corners of the lattice, these Majorana modes are indeed corner-localized and unambiguously signals the inversion-protected higher-order topology.

In Fig. 7 (d), we further list the parity data of this higher-order TSC phase at each high-symmetry momentum. To correctly calculate the parity data, we need to modify the Fourier transformation in Eq. 16 to $c_{\mathbf{R},l} = \sum_{\mathbf{k}} e^{i\mathbf{k}\cdot\mathbf{R}} c_{\mathbf{k},l}$. Then the inversion operator is found to be \mathbf{k} -dependent with

$$\mathcal{I} = \begin{pmatrix} 1 & & & \\ & e^{ik_y} & & \\ & & -1 & \\ & & & -e^{-ik_y} \end{pmatrix}. \quad (20)$$

To understand the parity data intuitively, we first note

that the system is essentially an array of x -directed Kitaev chain in the Kitaev limit $m \rightarrow 0$. Thus, the system has only one occupied band and the parity data is simply

$$[(+)\Gamma, (-)X, (+)Y, (-)M]. \quad (21)$$

Here $(+)\Gamma$ denotes one positive parity for the occupied band at Γ point. By turning on m , the system becomes dimerized along y -direction and leads to Brillouin zone (BZ) folding in the momentum space. As a result, the parity data at Y and M will be folded to Γ and M , respectively. We thus have $(+,+)\Gamma$ and $(-,-)X$. Meanwhile, $\tilde{Y} = (0, \frac{\pi}{2})$ transforms into $\tilde{Y}' = (0, -\frac{\pi}{2})$ under inversion, which is thus not an inversion-invariant momentum *before* the BZ folding. When the BZ folding happens, the BdG states at \tilde{Y}' and \tilde{Y} are folded together as the new Y point and the inversion operation switches between them as a σ_x operation. Therefore, the inversion eigenstates at Y after the BZ folding are necessarily the bonding and anti-bonding combinations of the states that are originally from \tilde{Y} and \tilde{Y}' . As a result, the occupied bands at Y must host an equal number of “+” and “-” parity eigenvalues after the BZ folding along k_y direction. A similar argument can be applied to the parity data at M . Therefore, we arrive at the following parity data for the higher-order TSC phase

$$[(+,+)\Gamma, (-,-)X, (+,-)Y, (+,-)M], \quad (22)$$

as shown in Fig. 7 (c).

3. $H_2(\mathbf{k})$ with $|t| < |m|$: A Weak TSC

When $|t| < |m|$, we take the Kitaev limit by setting $|t| \rightarrow 0$ instead. Then the Wannier orbitals will sit at the

center of the orange bonds m . To be specific, the system has one Wannier orbital at a non-maximal Wyckoff position $\mathbf{q} = (0, \frac{1}{4})$ and another at $\mathbf{q} = (0, \frac{3}{4})$. On the other hand, the two atomic sites sit at \mathbf{q}_{1a} and \mathbf{q}_{1c} , respectively. According to the Majorana counting rule, we have

$$\Delta_a = \Delta_c = -1, \quad \Delta_b = \Delta_d = 0, \quad (23)$$

and this phase is thus NOT higher-order topological.

In fact, the two Wannier orbitals inside one unit cell are inversion-symmetric around \mathbf{q}_{1a} . As a result, we can simultaneously move both Wannier orbitals to \mathbf{q}_{1a} in a symmetric and adiabatic way. Then the system is equivalent to a stacking of a κ_a at \mathbf{q}_{1a} and a κ_c at \mathbf{q}_{1c} , which does not satisfy higher-order condition in our recipe #2.

By counting the relative distance between atomic sites and the Wannier orbitals, we identify this phase as a weak TSC with a nontrivial polarization $\mathcal{P} = (0, \frac{1}{2})$. To verify this, we calculate the energy spectrum of the weak TSC phase with open boundary conditions in both directions. As shown in Fig. 7 (d) and its inset, this weak TSC phase indeed hosts a single Majorana flat band localized on its y -edge, as predicted by its polarization. We also show its parity data in Fig. 7 (e).

C. Displaced Stacking with Different Building Blocks

We can also stack different Kitaev building blocks in a displaced way to achieve higher-order topology. While it is difficult to prove a necessary and sufficient higher-order topological recipe for displaced stackings with inequivalent building blocks, we do emphasize that our Majorana counting rule still holds for diagnosing the higher-order topology. Hence, in the following, we will only provide a minimal example to demonstrate this stacking strategy and leave the proposal of a general recipe for future works. While hosting intrinsic higher-order topology, however, this minimal model is found to share the same parity data with a topologically trivial system. Therefore, this model cannot be diagnosed by the symmetry-eigenvalue-based classification for higher-order TSC, which represents an example of the beyond-indicator models.

1. Model Hamiltonian and Higher-order Topology

We now consider a displaced stacking with all four inequivalent building blocks: (i) one κ_a at \mathbf{q}_{1d} , (ii) one κ_b at \mathbf{q}_{1c} , (iii) one κ_c at \mathbf{q}_{1b} , and (iv) one κ_d at \mathbf{q}_{1a} . In this case, we have four atomic sites distributed at all four maximal Wyckoff positions and four Wannier orbitals coincide at \mathbf{q}_{1d} . Following the counting rule, we have

$$\Delta_a = \Delta_b = \Delta_c = -1, \quad \Delta_d = 3, \quad (24)$$

and thus the system is predicted to host higher-order topology.

To confirm this prediction, we consider a topologically equivalent model H_3 by symmetrically moving the Wannier orbitals at \mathbf{q}_{1d} to four non-maximal positions: $(\frac{1}{4}, \frac{1}{4})$, $(\frac{3}{4}, \frac{1}{4})$, $(\frac{1}{4}, \frac{3}{4})$, $(\frac{3}{4}, \frac{3}{4})$, following the procedure in Fig. 8 (a). We note that such deformation is adiabatic and should not spoil the higher-order topology since it only modifies the value of Δ_d to -1 .

In the Majorana representation, we can realize both the atomic and Wannier orbital configurations for H_3 by constructing a Majorana model shown in Fig. 8 (b). Notably, the unit cell now consists of four pairs of Majorana fermions (or equivalently, electron and hole pairs) at four inequivalent maximal Wyckoff positions. For convenience, we will use a two-component sublattice index $(i_x j_y)$ with $i, j \in \{A, B\}$ to label the four maximal Wyckoff positions. For example, we refer \mathbf{q}_{1a} as $(A_x A_y)$ and \mathbf{q}_{1b} as $(B_x A_y)$, which will be denoted as (AA) and (BA) for short. As shown in Fig. 8 (b), there are three inequivalent Majorana bonds for H_3 : (i) the strong green bonds t that decide the positions of Wannier orbitals; (ii) the weak (solid and dashed) purple dimer bonds m_y that remove the trivial edge modes on the y -edge; (iii) the weak (solid and dashed) red bonds m_x that remove the trivial edge modes on the x -edge. Just from the schematic plot in Fig. 8 (a), we already expect that there will be one single unpaired Majorana mode (shown by the red and blue circles) on both the top-right and bottom-left corners of an inversion-symmetric finite-size geometry.

Following Fig. 8 (b), the corresponding Majorana Hamiltonian H_3 consists of three parts: $h_{3,g}$ for the green bonds, $h_{3,p}$ for the purple bonds, and the $h_{3,r}$ for the red bonds. In the Majorana representation, we have

$$\begin{aligned} h_{3,g} &= it \sum_{\mathbf{R}} [\beta_{\mathbf{R},AA} \alpha_{\mathbf{R},BB} + \beta_{\mathbf{R},AB} \alpha_{\mathbf{R}+\mathbf{a}_y,BA} \\ &\quad + \beta_{\mathbf{R},BA} \alpha_{\mathbf{R}+\mathbf{a}_x,AB} + \beta_{\mathbf{R},BB} \alpha_{\mathbf{R}+\mathbf{a}_d,AA}], \\ h_{3,p} &= im_x \sum_{\mathbf{R}} [\beta_{\mathbf{R},AA} \beta_{\mathbf{R},BA} + \alpha_{\mathbf{R},AA} \alpha_{\mathbf{R}-\mathbf{a}_x,BA} \\ &\quad + \beta_{\mathbf{R},AB} \beta_{\mathbf{R},BB} + \alpha_{\mathbf{R},AB} \alpha_{\mathbf{R}-\mathbf{a}_x,BB}], \\ h_{3,r} &= im_y \sum_{\mathbf{R}} [\beta_{\mathbf{R},AA} \beta_{\mathbf{R},AB} + \alpha_{\mathbf{R},AA} \alpha_{\mathbf{R}-\mathbf{a}_y,AB} \\ &\quad + \beta_{\mathbf{R},BA} \beta_{\mathbf{R},BB} + \alpha_{\mathbf{R},BA} \alpha_{\mathbf{R}-\mathbf{a}_y,BB}], \end{aligned} \quad (25)$$

where we have defined $\mathbf{a}_d = \mathbf{a}_x + \mathbf{a}_y$ for simplicity. When transforming the Hamiltonian into momentum space, it is convenient to consider the Fourier transformations for the real-space Majorana operators. Take α -type Majorana operator as an example,

$$\alpha_{\mathbf{R},ij} = \sum_{\mathbf{k}} e^{i\mathbf{k}\cdot(\mathbf{R}+\mathbf{r}_{ij})} \alpha_{\mathbf{k},ij}, \quad (26)$$

where \mathbf{r}_{ij} is the displacement of the sublattice (ij) away from the unit-cell origin. The hermiticity of a Majorana

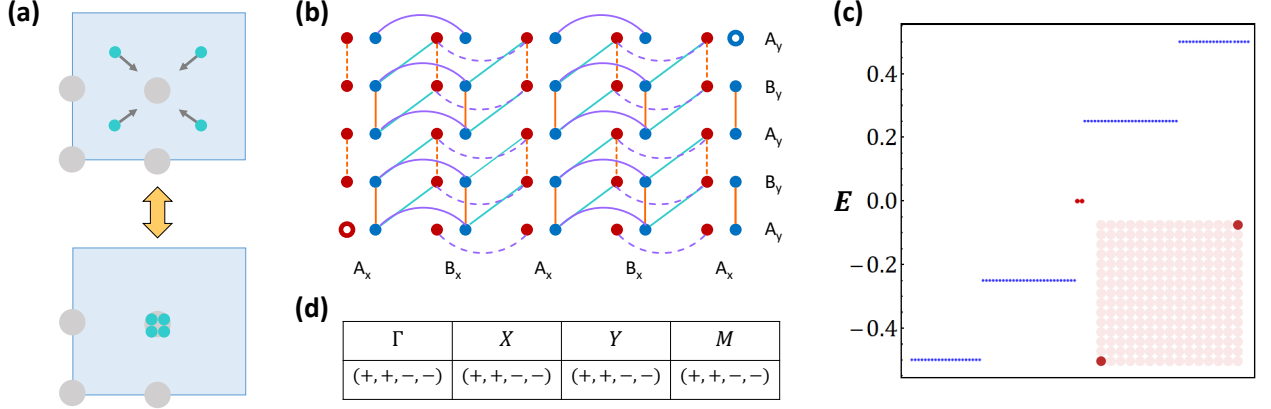


FIG. 8. Higher-order topology of displaced stacking model H_3 . In (a), we show the adiabatic process by symmetrically moving Wannier orbitals at different general Wyckoff positions to a maximal Wyckoff position. The Majorana representation of H_3 is shown in (b). The higher-order topology of H_3 is confirmed in (c) and its inset by plotting the energy spectrum on an open geometry. The parity data for H_3 is shown in (d), which is indistinguishable from that of a trivial BdG system. This establishes H_3 as an example that cannot be diagnosed by existing symmetry indicators.

operator requires

$$\alpha_{\mathbf{k},ij} = \alpha_{-\mathbf{k},ij}^\dagger. \quad (27)$$

We consider the following momentum-space Majorana basis

$$\Psi_M = (\alpha_{\mathbf{k},AA}, \beta_{\mathbf{k},AA}, \alpha_{\mathbf{k},BA}, \beta_{\mathbf{k},BA}, \alpha_{\mathbf{k},AB}, \beta_{\mathbf{k},AB}, \alpha_{\mathbf{k},BB}, \beta_{\mathbf{k},BB})^T, \quad (28)$$

$$H_3(\mathbf{k}) = \begin{pmatrix} 0 & 0 & im_x e^{i\frac{k_x}{2}} & 0 & im_y e^{i\frac{k_y}{2}} & 0 & 0 & -ite^{i\frac{k_x+k_y}{2}} \\ 0 & 0 & 0 & im_x e^{-i\frac{k_x}{2}} & 0 & im_y e^{-i\frac{k_y}{2}} & ite^{-i\frac{k_x+k_y}{2}} & 0 \\ -im_x e^{-i\frac{k_x}{2}} & 0 & 0 & 0 & 0 & -ite^{i\frac{k_x+k_y}{2}} & im_y e^{i\frac{k_y}{2}} & 0 \\ 0 & -im_x e^{i\frac{k_x}{2}} & 0 & 0 & ite^{-i\frac{k_x+k_y}{2}} & 0 & 0 & im_y e^{-i\frac{k_y}{2}} \\ -im_y e^{-i\frac{k_y}{2}} & 0 & 0 & -ite^{i\frac{k_x+k_y}{2}} & 0 & 0 & im_x e^{i\frac{k_x}{2}} & 0 \\ 0 & -im_y e^{i\frac{k_y}{2}} & ite^{-i\frac{k_x+k_y}{2}} & 0 & 0 & 0 & 0 & im_x e^{-i\frac{k_x}{2}} \\ 0 & -ite^{i\frac{k_x+k_y}{2}} & -im_y e^{-i\frac{k_y}{2}} & 0 & -im_y e^{-i\frac{k_y}{2}} & 0 & 0 & 0 \\ ite^{-i\frac{k_x+k_y}{2}} & 0 & 0 & -im_y e^{i\frac{k_y}{2}} & 0 & -im_x e^{i\frac{k_x}{2}} & 0 & 0 \end{pmatrix} \quad (29)$$

Interestingly, H_3 can be diagonalized analytically and we find that the energy eigenvalues are completely \mathbf{k} -independent:

$$E = \pm \sqrt{t^2 + (m_x \pm m_y)^2}. \quad (30)$$

To further clarify the higher-order nature of H_3 , we consider an inversion-symmetric open geometry for H_3 and calculate the energy spectrum with $t = 1$ and $m_x = m_y = 0.5$. As shown in Fig. 8 (c) and its inset, we confirm the existence of a pair of corner-localized Majorana zero modes, which agrees with the prediction

under which the Hamiltonian is given by

from the counting rule.

2. Beyond Symmetry Indicators

We also calculate the parity data for the higher-order TSC phase of $H_3(\mathbf{k})$, which is shown in Fig. 8 (d). The

inversion operator is given by

$$\mathcal{I} = \tau_z \otimes \begin{pmatrix} 1 & & & \\ & e^{ik_x} & & \\ & & e^{ik_y} & \\ & & & e^{i(k_x+k_y)} \end{pmatrix} \quad (31)$$

in the fermion basis

$$\Phi_F = (c_{\mathbf{k},AA}, c_{\mathbf{k},BA}, c_{\mathbf{k},AB}, c_{\mathbf{k},BB}, c_{-\mathbf{k},AA}^\dagger, c_{-\mathbf{k},BA}^\dagger, c_{-\mathbf{k},AB}^\dagger, c_{-\mathbf{k},BB}^\dagger)^T. \quad (32)$$

Interestingly, H_3 has an equal number of “+” and “-” parity eigenvalues for every high-symmetry points. To understand this parity data, we note that m_x and m_y are essentially dimer bonds that lead to unit-cell enlargement. Therefore, the BZ with finite $m_{x,y}$ is actually folded in both k_x and k_y directions, in comparison to the original BZ without the dimers. Similar to the double-stacking model $H_2(\mathbf{k})$, the inversion eigenstates for the new high-symmetry momenta after the BZ folding are essentially the bonding and anti-bonding combinations of energy eigenstates at these momenta that transform from one to another under inversion. As a result, we will always have an equal number of energy eigenstates with “+” and “-” parity eigenvalues at all high-symmetry momenta.

Now let us consider a topologically trivial Kitaev superconductor with two s -like Wannier orbitals and two p -like Wannier orbitals at \mathbf{q}_{1a} . While this system is guaranteed to have no topological boundary feature, it does share the SAME parity data with the above higher-order TSC model H_3 . In other words, this trivial model CANNOT be distinguished from H_3 via a symmetry-eigenvalue-based diagnosis (i.e. symmetry indicators). This is why we call H_3 a “beyond-indicator” model.

To understand the possible limitation of the symmetry indicators, we emphasize that most symmetry-indicator-based classification schemes [56, 57, 59–62] have assumed \mathbf{k} -independent matrix representations for the target symmetries. An example that satisfies this assumption is simply our face-to-face stacking model H_1 with an inversion operation $\mathcal{I} = \tau_z \otimes \mathbb{1}_3$.

However, this requirement cannot be always fulfilled for a general BdG system with sublattice degrees of freedom, which is exactly the case for our H_3 model. Specifically, when the system has atomic sites at \mathbf{q}_{1i} for $i = b, c, d$, it is usually not possible to “gauge out” the momentum-dependent phase factor in the matrix representation of \mathcal{I} . In fact, our model H_2 in Sec. IV B is also a beyond-indicator model, which can be checked easily. Despite this limitation of symmetry indicators, we emphasize that our Majorana counting rule does predict the correct higher-order topology for both beyond-indicator models. This is simply because our counting rule is essentially a real-space diagnosis and thus does not reply on the explicit form of momentum-space representation for a given crystalline symmetry.

From a different perspective, our displaced stacking strategy offers a general construction scheme for beyond-indicator models with momentum-dependent symmetry representations. We emphasize that a complete topological theory for BdG systems must be able to explain all of the beyond-indicator models constructed via the displaced stacking scheme.

V. A CONJECTURE OF UNIVERSAL TOPOLOGICAL DIAGNOSIS

The Majorana counting rule has been proved quite successful in diagnosing higher-order topology for general Kitaev superconductors. However, a real-world superconductor does not necessarily (and most unlikely) admit a maximally localized Wannier description. Therefore, for the practical purpose, it is natural to ask whether it is possible to go beyond the Kitaev limit and extend this diagnosis to a general Wannierizable 2d BdG system. We hope to initiate some efforts along this direction by first conjecturing that

- A general 2d Wannierizable class D BdG system with inversion symmetry can always be adiabatically deformed into a Kitaev limit.

This conjecture aims at establishing an exact mapping between a general Wannierizable superconductor and a corresponding Kitaev superconductor through adiabatic evolutions. If this conjecture is true, we will be able to diagnose the higher-order topology of any Wannierizable superconductor, following a diagnostic procedure in Fig. 9.

In the following, we briefly go through the proposed procedure for this conjectured universal diagnosis:

- **Step 1:** Given a 2d class D superconductor with inversion symmetry, first check if its Wannierizability. If the Wannier obstruction is fragile, remove it. If not, characterize the system as a stable topological superconductor, where the term “stable” is defined to describe the robustness of Wannier obstruction.
- **Step 2:** If there is no stable Wannier obstruction, connect the system to a Kitaev superconductor adiabatically. This procedure can always be done if our conjecture is true.
- **Step 3:** Extract the numbers of Wannier orbitals and atomic sites at each maximal Wyckoff positions. Calculate Majorana counting numbers.
- **Step 4:** If the counting numbers are non-trivial, the system is a higher-order TSC. If not, the system could be either a trivial superconductor or a weak TSC, depending on the explicit value of polarization \mathcal{P} .

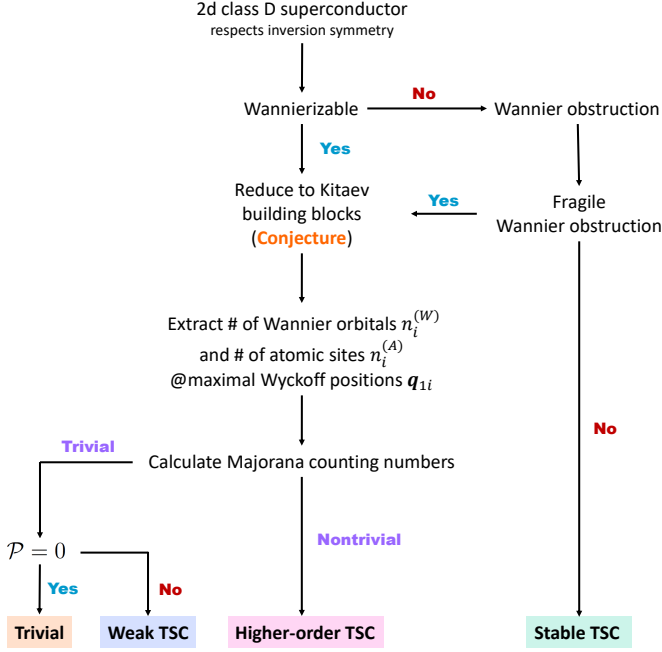


FIG. 9. The flow diagram of our conjectured universal diagnosis for general 2d higher-order TSCs.

While rigorously proving our conjecture seems difficult and is beyond the scope of current work, we do have a strong belief that our conjecture and the proposed diagnosis should hold for general Wannierizable superconductors.

To demonstrate our conjectured universal diagnosis, in the next section, we will discuss a known higher-order TSC model in the literature. We will first show that this model actually hosts fragile Wannier obstruction and is definitely beyond the Kitaev limit. Nevertheless, we will follow the universal diagnosis to first remove the Wannier obstruction and connect the new Wannierizable system to a well-defined Kitaev superconductor. This allows us to understand the origin of higher-order topology for the original model through a very simple Majorana counting, which clearly verifies of our conjectured diagnosis.

VI. APPLICATION TO A REALISTIC HIGHER-ORDER TOPOLOGICAL SUPERCONDUCTOR

Let us now consider a realistic higher-order TSC that has been discussed in the literatures [30, 51]. This model consists of one $p + ip$ chiral TSC and another $p - ip$ chiral TSC [30], and is thus a superconducting version of the “shift insulator” in Ref. [70]. We first present a minimal tight-binding model of such system and explicitly show the existence of Majorana corner modes by deriving an effective edge theory analytically. We then calculate its Wilson loop spectrum to confirm the inversion-protected

Wannier obstruction, manifested in the nontrivial Wilson loop winding. However, such Wilson loop winding can be trivialized if we couple the system with additional Wannier orbitals, which thus confirms the fragility of Wannier obstruction [71]. By matching the stacked chiral TSC model with a superposition of Kitaev building blocks, we provide an understanding of its higher-order topology with the help of our Majorana counting rule.

A. Model Hamiltonian for Stacked Chiral TSCs

The minimal tight-binding model for two decoupled chiral TSC is given by

$$H_4^{(0)} = [m_0 + m_1(\cos k_x + \cos k_y)]\Gamma_5 + v(\sin k_x\Gamma_1 + \sin k_y\Gamma_2) \quad (33)$$

where we have defined the generator of 4×4 Γ matrices as

$$\begin{aligned} \Gamma_1 &= \tau_x \otimes \sigma_0, & \Gamma_2 &= \tau_y \otimes \sigma_0, & \Gamma_3 &= \tau_z \otimes \sigma_x, \\ \Gamma_4 &= \tau_x \otimes \sigma_y, & \Gamma_5 &= \tau_z \otimes \sigma_z, \end{aligned} \quad (34)$$

These Γ matrices satisfy an anti-commutation relation $\{\Gamma_i, \Gamma_j\} = 2\delta_{ij}$ for $i, j \in \{1, 2, 3, 4, 5\}$. The other ten Γ matrices can be generated by $\Gamma_{jk} = \frac{1}{2i}[\Gamma_j, \Gamma_k]$ for $j \neq k$.

Note that $H_4^{(0)}$ is block-diagonal and can be written as a direct sum of a $p + ip$ chiral TSC h_+ and another $p - ip$ chiral TSC h_- . In particular,

$$h_{\pm}(\mathbf{k}) = \pm[m_0 + m_1(\cos k_x + \cos k_y)]\tau_z + v(\sin k_x\tau_x + \sin k_y\tau_y). \quad (35)$$

We have defined the particle-hole symmetry as $\Xi = \Gamma_1\mathcal{K}$ and the inversion symmetry as $\mathcal{I} = \Gamma_5$, where \mathcal{K} is the complex conjugation.

We now consider adding symmetry-allowed perturbation $H_4^{(1)}$ to remove the accidental edge modes of $H_4^{(0)}$. To be specific, we hope to find a constant matrix A to preserve both inversion \mathcal{I} and the particle-hole symmetry Ξ . Namely, A should satisfy (i) $\{A, \Xi\} = 0$; (ii) $[A, \mathcal{I}] = 0$. We find the following choice of A :

$$A = \{\Gamma_5, \Gamma_{12}, \Gamma_{14}, \Gamma_{24}\}, \quad (36)$$

which inspires us to define

$$H_4^{(1)} = g_1\Gamma_{14} + g_2\Gamma_{24} + g_3\Gamma_{12}, \quad (37)$$

where we have ignored Γ_5 in $H_4^{(1)}$ since it is already contained in $H_4^{(0)}$. The complete Hamiltonian for stacked chiral TSC is thus $H_4 = H_4^{(0)} + H_4^{(1)}$.

B. Higher-order Topology from a Boundary Perspective

Before providing any numerical results for H_4 , we first demonstrate the origin of its higher-order topology from

an analytical boundary perspective. We will derive an effective analytical boundary theory for H_4 in a disk geometry and explicitly show the existence of corner-localized Majorana zero modes, similar to the approaches in Ref. [51, 52].

We first treat $H_4^{(1)}$ as a small perturbation and expand h_{\pm} around Γ point. This leads to an effective Hamiltonian around Γ for both chiral TSC block,

$$h_{\pm}^{\Gamma}(\mathbf{k}) = \pm[\tilde{m}_0 - \tilde{m}_1(k_x^2 + k_y^2)]\tau_z + v(k_x\tau_x + k_y\tau_y), \quad (38)$$

where we have defined $\tilde{m}_0 = (m_0 + 2m_1)$ and $\tilde{m}_1 = \frac{m_1}{2}$. In the polar coordinate $r = \sqrt{x^2 + y^2}$ and $\theta = \tan^{-1} \frac{y}{x}$, we have $k_{\pm} = e^{\pm i\theta}(k_r \pm ik_{\theta})$ with $k_r = -\partial_r$ and $k_{\theta} = -\frac{i}{r}\partial_{\theta}$. Up to $\mathcal{O}(k)$, h_{\pm}^{Γ} can be written as

$$h_{\pm}^{\Gamma}(r, \theta) = \begin{pmatrix} \pm\tilde{m}_0 & ve^{-i\theta}(-i\partial_r - \frac{1}{r}\partial_{\theta}) \\ ve^{i\theta}(-i\partial_r + \frac{1}{r}\partial_{\theta}) & \mp\tilde{m}_0 \end{pmatrix}. \quad (39)$$

We consider a disk geometry with a radius R and solve for the Majorana wavefunction that is exponentially localized at $r = R$. In the large R limit, we find a single Majorana solution ψ_{\pm} for h_{\pm} :

$$\psi_{\pm}(l, r, \theta) = \mathcal{N}_{\psi} e^{\pm \frac{m}{v}(r-R)} e^{il\theta} \begin{pmatrix} e^{-\frac{i}{2}(\theta \pm \frac{\pi}{2})} \\ e^{\frac{i}{2}(\theta \pm \frac{\pi}{2})} \end{pmatrix} \quad (40)$$

with $l \in \mathbb{Z}$ and a normalization factor \mathcal{N}_{ψ} . The energy dispersion for $\psi_{\pm}(l, r, \theta)$ is

$$E_{\pm, l} = \pm \frac{vl}{r}. \quad (41)$$

Therefore, ψ_+ and ψ_- represent a pair of chiral Majorana edge modes propagating in the opposite directions. Now we are ready to project the perturbation $H_4^{(1)}$ onto the chiral Majorana basis and we arrive at an effective edge Hamiltonian

$$H_{\text{edge}} = \frac{vl}{r}\sigma_z - (g_1 \sin \theta - g_2 \cos \theta)\sigma_y. \quad (42)$$

Therefore, the edge spectrum is given by

$$E_{\text{edge}} = \pm \sqrt{\left(\frac{vl}{r}\right)^2 + (g_1^2 + g_2^2) \sin(\theta - \theta_0)}, \quad (43)$$

where we have defined $\theta_0 = \tan^{-1} \frac{g_2}{g_1}$. Clearly, the boundary gap closes for the chiral Majorana modes with $l = 0$ only when $\theta = \theta_0$ and $\theta = \theta_0 + \pi$. Therefore, the system hosts a pair of corner-localized Majorana zero modes at these two inversion-related angles and is thus higher-order topological by definition.

C. Fragile Wannier Obstruction

We now consider placing H_4 on a 15×15 lattice and calculate its energy spectrum. As shown in Fig. 10 (a)

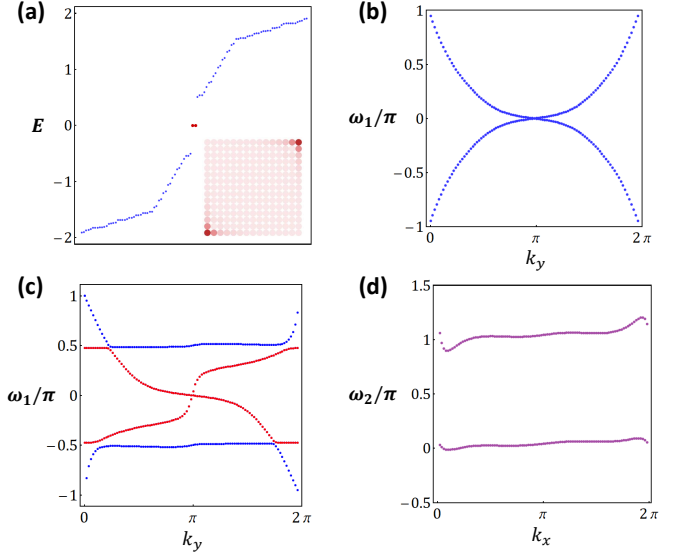


FIG. 10. We numerically verify in (a) and the inset that the stacked chiral TSC model H_4 is higher-order topological by calculating its energy spectrum on an open geometry and confirm its corner-localized Majorana zero modes. In (b), we calculate the 1d x -directed Wilson loop spectrum $\omega_1(k_y)$. ω_1 is found to host a nontrivial winding pattern which directly implies the existence of Wannier obstruction. In (c), we explicitly demonstrate the fragility of Wannier obstruction by coupling H_4 to a Wannierizable system H_w and thus “unwind” the Wilson loop pattern. In (d), we calculate the y -directed nested Wilson loop $\omega_2(k_x)$ for the red Wannier band sector in (c).

and its inset, there exists a pair of corner-localized Majorana zero modes, which establishes H_4 as a higher-order TSC. In particular, the model parameters are chosen to be $m_0 = -m_1 = 3$ and $g_1 = g_2 = 0.5$. According to our boundary theory, the corner Majorana modes are predicted to be localized on the inversion-related boundary positions, which are characterized by the polar angle $\theta = \theta_0 = \tan^{-1} 1 = \frac{\pi}{4}$ and $\theta = \frac{5\pi}{4}$. This agrees well with our numerical findings shown in the inset of Fig. 10 (a).

The Wannier obstruction of H_4 is clearly revealed by calculating the bulk Wilson loop spectrum $\omega_1^x(k_y)$, which is often known as the “Wannier band spectrum” [25]. As shown in Fig. 10 (b), the Wilson loop $\omega_1^x(k_y)$ exhibits a nontrivial winding pattern which prohibits a symmetric and localized Wannier representation for H_4 . Such winding pattern is relatively robust by itself due to the inversion-symmetry protection [72].

However, if we couple H_4 with another Wannierizable system H_w , we can unwind the Wilson loop (gap out the Wannier bands) to recover the Wannierizability [34, 73]. To achieve this, we consider a composite system H_5 , with

$$H_5 = \begin{pmatrix} H_4 & h_c \\ h_c^\dagger & H_w \end{pmatrix}. \quad (44)$$

We have constructed H_w by placing one Wannier orbital at $\mathbf{q}_1 = (\frac{1}{4}, \frac{1}{4})$ and another Wannier orbital at $\mathbf{q}_2 = (-\frac{1}{4}, -\frac{1}{4})$. Note that one can symmetrically move both Wannier orbitals to \mathbf{q}_{1a} without spoiling the adiabaticity. Therefore, H_w is adiabatically equivalent to stacking two building blocks κ_a at \mathbf{q}_{1a} , which is both Wannierizable and topologically trivial.

Specifically, we consider the BdG basis $\Phi_w = (c_{1,\mathbf{k}}, c_{1,-\mathbf{k}}^\dagger, c_{2,\mathbf{k}}, c_{2,-\mathbf{k}}^\dagger)^T$ for H_w , where $c_{i,\mathbf{k}}$ annihilates an electron at \mathbf{q}_i for $i = 1, 2$. Then H_w and the coupling matrix h_c are given by

$$H_w = t \begin{pmatrix} \epsilon_0 & 0 & f(\mathbf{k})^2 & 0 \\ 0 & -\epsilon_0 & 0 & -f(\mathbf{k})^2 \\ [f(\mathbf{k})^*]^2 & 0 & \epsilon_0 & 0 \\ 0 & -[f(\mathbf{k})^*]^2 & 0 & -\epsilon_0 \end{pmatrix},$$

$$h_c = g_c \begin{pmatrix} f(\mathbf{k})^* & 0 & f(\mathbf{k}) & 0 \\ 0 & -f(\mathbf{k})^* & 0 & -f(\mathbf{k}) \\ 0 & 0 & 0 & 0 \\ 0 & 0 & 0 & 0 \end{pmatrix}. \quad (45)$$

where we have defined $f(\mathbf{k}) = e^{\frac{i}{4}(k_x + k_y)}$.

For our purpose, we choose a large $\epsilon_0 = 30$ such that the BdG bands of H_w stay away from the Fermi level. We also choose $t = 0.5$ and $g_c = 4$ and calculate the x -directed Wilson loop for the composite system H_5 . As shown in Fig. 10 (c), now the Wannier bands are gapped out and can be separated into two disjoint segments, which are plotted in red and blue, respectively. This unwinding pattern directly suggests that the previous Wannier obstruction for H_4 is indeed removed, which is a hallmark for fragile Wannier obstruction.

D. Nested Wilson Loop, Parity Data, and Majorana Counting

To perform our universal diagnosis, note that it is generally challenging to find an adiabatic path to connect the Wannierizable composite system H_5 and a corresponding Kitaev superconductor. Consequently, we will try to establish such adiabatic connection in an indirect way. We will explicitly show that both its (nested) Wilson loops [25] and the parity data indicate a unique decomposition of H_4 in terms of the Kitaev building blocks. This decomposition allows us to explain the higher-order topological origin of the stacked chiral TSC model H_4 with our Majorana counting rule.

Physically, the value of Wilson loops $\omega_x^x(k_y)$ is the expectation value of x -position operator \hat{x} in the Wannier representation. Therefore, a gapped Wannier band spectrum in Fig. 8 (c) directly implies the existence of two spatially separated electron clouds along x -direction within the unit cell. To be specific, the red (blue) Wannier bands correspond to an electron cloud localized around $x = 0$ ($x = \frac{1}{2}$).

	Γ	X	Y	M
H_5	(+, +, +, -)	(-, -, +, -)	(-, -, +, -)	(-, -, +, -)
$p @ \mathbf{q}_{1a}$	-	-	-	-
$s @ \mathbf{q}_{1b}$	+	-	+	-
$s @ \mathbf{q}_{1c}$	+	+	-	-
$s @ \mathbf{q}_{1d}$	+	-	-	+

TABLE I. This table shows the decomposition of the composite system H_5 with respect to Kitaev building blocks, from the perspective of parity data. For the parity data of H_5 , the data in red (blue) color shows the contribution from H_4 (H_w). About the notation of the decomposition, for example, we have use “ $p @ \mathbf{q}_{1a}$ ” to denote a Kitaev building block with a p -like orbital sitting at \mathbf{q}_{1a} .

To further extract the position information for the electron clouds along y -direction, we calculate the nested Wilson loop $\omega_2^y(k_x)$ for each colored group of Wannier bands. As shown in Fig. 8 (d), we find two nested Wannier bands localized around $\omega_2^y = 0$ and $\omega_2^y = \frac{1}{2}$, respectively. Physically, this implies that the red electron cloud at $x = 0$ can be further divided into two separated smaller electron clouds along y -direction. In particular, one cloud sits around $\mathbf{q}_{1a} = (0, 0)$ and the other locates at $\mathbf{q}_{1c} = (0, \frac{1}{2})$. A similar nested Wilson loop calculation can be performed for the blue Wannier band sector, which shows a similar spectrum to Fig. 8 (d). This suggests the existence of two electron clouds at \mathbf{q}_{1b} and \mathbf{q}_{1d} , respectively.

However, one should be careful about interpreting the (nested) Wilson loop results as the actual positions of Wannier orbitals in real-space. Since the (nested) Wilson loops are essentially projected position operators for a specific (Wannier) band sector, the projected \hat{x} and \hat{y} operators do not generally commute. For example, we could calculate the y -directed Wilson loop ω_1^y and the x -directed nested Wilson loop ω_2^x , instead of the ω_1^x and ω_2^y that we have calculated. Then it is possible that $(\omega_1^x, \omega_2^y) \neq (\omega_1^y, \omega_2^x)$. While this ambiguity does not exist for our present model, an example with this issue does exist and was addressed in Ref. [25].

To further rule out the ambiguity of the Wilson loop calculations, we further calculate the parity data for the composite system H_5 , as shown in Table I. In particular, we can trust the parity data for H_5 simply because it does have momentum-independent inversion representation. To demonstrate, we have highlighted the parity contribution for H_4 in red and that for the Wannierizable system H_w in blue. We note that the parity data for H_5 is the same as that for a face-to-face stacking of one p -like orbital at \mathbf{q}_{1a} and three s -like orbital at the other three maximal Wyckoff positions, as shown in Table I.

It is easy to see that such parity data decomposition is indeed *unique*. Then the parity data and the Wilson loop calculations reach a consistent decomposition relation for H_5 that

$$H_5 \equiv \kappa_a(p) \oplus \kappa_b(s) \oplus \kappa_c(s) \oplus \kappa_d(s), \quad (46)$$

where we have denote a κ_i with an α -type orbital as $\kappa_i(\alpha)$. Here “ \equiv ” denotes the adiabatic equivalence relation between the two systems and “ \oplus ” denotes the stacking operation of Kitaev building blocks.

Recall that $H_w \equiv \kappa_a(s) \oplus \kappa_a(p)$. Then we have

$$H_4 \equiv H_5 \ominus H_w \equiv \kappa_b(s) \oplus \kappa_c(s) \oplus \kappa_d(s) \ominus \kappa_a(s). \quad (47)$$

Namely, H_4 is equivalent to a stacking of $\kappa_{b,c,d}$ with an additional “subtraction \ominus ” of κ_a . From the Majorana counting rule, we have shown that the face-to-face stacking of $\kappa_{b,c,d}$ is higher-order topological but κ_a is not. As a result, the stacked chiral TSC model H_4 is then naturally higher-order topological, which clearly verifies our conjectured universal diagnosis.

For the case of \mathbf{k} -independent inversion operators, we emphasize that our building block analysis shows that the parity data uniquely indicates the higher-order topological phase. Specifically, the higher order-topological phase is characterized by an odd number of “double band inversions” [i.e. $(-, -)$ pattern] at the same high-symmetry momentum, which is indeed the case for both H_1 and H_4 . Assuming the conjecture in Sec. V is true, this provides a simple form for the topological invariant for higher-order superconductors with \mathbf{k} -independent inversion representations that can be computed directly from the parity pattern without computing Wannier functions or Wilson loops. [NOTE: for the record, we made this conjecture before and dropped it in the arxiv version of Ref. [51] because we were not sure and this form of the invariant does not exist in the literature]

VII. CONCLUSION

To conclude, we have defined Kitaev limit as a key concept for constructing and diagnosing Wannierizable higher-order topological superconductors in any spatial dimension. Different from the symmetry-indicator-based classifications, our approach starts from a complete set of real-space Kitaev building blocks, by stacking which various higher-order TSC phases can be systematically achieved. Notably, some Kitaev superconductors with higher-order topology have \mathbf{k} -dependent symmetry representations, which are beyond the detection of existing symmetry indicators. Nevertheless, we have proposed a simple but powerful Majorana counting rule that diagnoses higher-order topology for all Kitaev superconductors. For general Wannierizable superconductors, we

have conjectured a universal diagnostic procedure for determining higher-order topology and discussed a realistic example to show how this universal diagnosis works in general.

Starting from our theory, it is quite straightforward to extend our building block construction to superconductors with other crystalline group symmetries. In particular, for such extension to a given space group, one only needs to identify a corresponding set of Kitaev building blocks and slightly modify the Majorana counting rule accordingly, which simply follows the procedure defined in Sec. III. Furthermore, similar construction strategy can also applied for designing and diagnosing higher-order topological Kitaev superconductors in class DIII with spinful time-reversal symmetry [74]. Therefore, our theory indeed provides a general framework for constructing and understanding higher-order TSC from the real-space perspective.

Recently, there is an interesting proposal about using “pairing obstruction” instead of Wannier obstruction to understand the topological behavior of superconductors [75]. Following the original definition in Ref. [76], the pairing obstruction is characterized by a real-space two-point function $g_{\mathbf{r}\mathbf{r}'}$ that describes the spatial profile of the Cooper pairs. In particular, a BdG system is pairing obstructed and thus proposed to be topological if $g_{\mathbf{r}\mathbf{r}'}$ falls off as a polynomial function of $|\mathbf{r} - \mathbf{r}'|$. In other words, the pairing obstruction occurs if the Fourier transform of $g_{\mathbf{r}\mathbf{r}'}$ is singular. We note that our Kitaev building blocks $\kappa_{b,c,d}$ do have similar pairing obstructions because of the inter-atomic-site Majorana bonds. Therefore, it is easy to check that all of the Kitaev superconductors with higher-order topology in our work are indeed pairing obstructed.

At this moment, it is still unknown that whether a mathematical description of topological invariants in momentum space can be formulated to correctly diagnose all higher-order TSCs. Nevertheless, if such theory indeed exists, all the examples presented in this work (especially the beyond-indicator models) manifest themselves as a touchstone for checking the completeness of the topological classification scheme.

ACKNOWLEDGMENTS

RXZ is grateful to DinhDuy Vu, Jiabin Yu, and especially Yi-Ting Hsu and Sheng-Jie Huang for helpful discussions. This work is supported by the Laboratory for Physical Sciences and Microsoft. RXZ acknowledges a JQI Postdoctoral Fellowship. JS was supported by the nsf-dmr1555135 (CAREER). This research was supported in part (through helpful discussions at KITP) by the National Science Foundation under Grant No. NSF PHY-1748958.

-
- [1] R. B. Laughlin, *Phys. Rev. Lett.* **50**, 1395 (1983).
- [2] D. J. Thouless, M. Kohmoto, M. P. Nightingale, and M. den Nijs, *Phys. Rev. Lett.* **49**, 405 (1982).
- [3] J. E. Avron, R. Seiler, and B. Simon, *Phys. Rev. Lett.* **51**, 51 (1983).
- [4] M. R. Zirnbauer, *Journal of Mathematical Physics* **37**, 4986 (1996).
- [5] A. Altland and M. R. Zirnbauer, *Phys. Rev. B* **55**, 1142 (1997).
- [6] C. L. Kane and E. J. Mele, *Phys. Rev. Lett.* **95**, 146802 (2005).
- [7] A. Y. Kitaev, *Physics-Uspekhi* **44**, 131 (2001).
- [8] C. Nayak, S. H. Simon, A. Stern, M. Freedman, and S. Das Sarma, *Rev. Mod. Phys.* **80**, 1083 (2008).
- [9] X. Chen, Z.-C. Gu, Z.-X. Liu, and X.-G. Wen, *Phys. Rev. B* **87**, 155114 (2013).
- [10] T. Senthil, *Annual Review of Condensed Matter Physics* **6**, 299 (2015).
- [11] C.-K. Chiu, J. C. Y. Teo, A. P. Schnyder, and S. Ryu, *Rev. Mod. Phys.* **88**, 035005 (2016).
- [12] M. Z. Hasan and C. L. Kane, *Rev. Mod. Phys.* **82**, 3045 (2010).
- [13] X.-L. Qi and S.-C. Zhang, *Rev. Mod. Phys.* **83**, 1057 (2011).
- [14] L. Fu, *Phys. Rev. Lett.* **106**, 106802 (2011).
- [15] T. H. Hsieh, H. Lin, J. Liu, W. Duan, A. Bansil, and L. Fu, *Nature Communications* **3**, 982 (2012).
- [16] Y. Ando and L. Fu, *Annual Review of Condensed Matter Physics* **6**, 361 (2015).
- [17] C.-X. Liu, R.-X. Zhang, and B. K. VanLeeuwen, *Phys. Rev. B* **90**, 085304 (2014).
- [18] Z. Wang, A. Alexandradinata, R. J. Cava, and B. A. Bernevig, *Nature* **532**, 189 EP (2016).
- [19] P.-Y. Chang, O. Erten, and P. Coleman, *Nature Physics* **13**, 794 EP (2017).
- [20] T. Thonhauser and D. Vanderbilt, *Phys. Rev. B* **74**, 235111 (2006).
- [21] A. A. Soluyanov and D. Vanderbilt, *Phys. Rev. B* **83**, 035108 (2011).
- [22] B. Bradlyn, L. Elcoro, J. Cano, M. G. Vergniory, Z. Wang, C. Felser, M. I. Aroyo, and B. A. Bernevig, *Nature* **547**, 298 (2017).
- [23] We note that there are multiple definitions of “higher-order topology” in the community. The higher-order topological systems in our work are bulk topological phases with necessary crystalline symmetry protections and thus admit a higher-order bulk-boundary correspondence.
- [24] W. A. Benalcazar, B. A. Bernevig, and T. L. Hughes, *Phys. Rev. B* **96**, 245115 (2017).
- [25] W. A. Benalcazar, B. A. Bernevig, and T. L. Hughes, *Science* **357**, 61 (2017).
- [26] J. Langbehn, Y. Peng, L. Trifunovic, F. von Oppen, and P. W. Brouwer, *Phys. Rev. Lett.* **119**, 246401 (2017).
- [27] Z. Song, Z. Fang, and C. Fang, *Phys. Rev. Lett.* **119**, 246402 (2017).
- [28] F. Schindler, A. M. Cook, M. G. Vergniory, Z. Wang, S. S. P. Parkin, B. A. Bernevig, and T. Neupert, *Science Advances* **4** (2018).
- [29] E. Khalaf, H. C. Po, A. Vishwanath, and H. Watanabe, *Phys. Rev. X* **8**, 031070 (2018).
- [30] E. Khalaf, *Phys. Rev. B* **97**, 205136 (2018).
- [31] G. van Miert and C. Ortix, *Phys. Rev. B* **98**, 081110 (2018).
- [32] Z. Wang, B. J. Wieder, J. Li, B. Yan, and B. A. Bernevig, *Phys. Rev. Lett.* **123**, 186401 (2019).
- [33] N. Varnava and D. Vanderbilt, *Phys. Rev. B* **98**, 245117 (2018).
- [34] B. J. Wieder and B. A. Bernevig, arXiv preprint arXiv:1810.02373 (2018).
- [35] Y. Xu, Z. Song, Z. Wang, H. Weng, and X. Dai, *Phys. Rev. Lett.* **122**, 256402 (2019).
- [36] C. Yue, Y. Xu, Z. Song, H. Weng, Y.-M. Lu, C. Fang, and X. Dai, *Nature Physics* **15**, 577 (2019).
- [37] R.-X. Zhang, F. Wu, and S. D. Sarma, (2019), arXiv:1910.11906 [cond-mat.mes-hall].
- [38] F. Schindler, Z. Wang, M. G. Vergniory, A. M. Cook, A. Murani, S. Sengupta, A. Y. Kasumov, R. Deblock, S. Jeon, I. Drozdov, H. Bouchiat, S. Guéron, A. Yazdani, B. A. Bernevig, and T. Neupert, *Nature Physics* **14**, 918 (2018).
- [39] H. C. Po, A. Vishwanath, and H. Watanabe, *Nature Communications* **8**, 50 (2017).
- [40] S. Ono and H. Watanabe, *Phys. Rev. B* **98**, 115150 (2018).
- [41] Q. Wang, C.-C. Liu, Y.-M. Lu, and F. Zhang, *Phys. Rev. Lett.* **121**, 186801 (2018).
- [42] Z. Yan, F. Song, and Z. Wang, *Phys. Rev. Lett.* **121**, 096803 (2018).
- [43] T. Liu, J. J. He, and F. Nori, *Phys. Rev. B* **98**, 245413 (2018).
- [44] Y. Wang, M. Lin, and T. L. Hughes, *Phys. Rev. B* **98**, 165144 (2018).
- [45] H. Shapourian, Y. Wang, and S. Ryu, *Phys. Rev. B* **97**, 094508 (2018).
- [46] C.-H. Hsu, P. Stano, J. Klinovaja, and D. Loss, *Phys. Rev. Lett.* **121**, 196801 (2018).
- [47] N. Bultinck, B. A. Bernevig, and M. P. Zaletel, *Phys. Rev. B* **99**, 125149 (2019).
- [48] R.-X. Zhang, W. S. Cole, and S. Das Sarma, *Phys. Rev. Lett.* **122**, 187001 (2019).
- [49] R.-X. Zhang, W. S. Cole, X. Wu, and S. Das Sarma, *Phys. Rev. Lett.* **123**, 167001 (2019).
- [50] X. Wu, X. Liu, R. Thomale, and C.-X. Liu, arXiv preprint arXiv:1905.10648 (2019).
- [51] Y.-T. Hsu, W. S. Cole, R.-X. Zhang, and J. D. Sau, arXiv preprint arXiv:1904.06361 (2019).
- [52] R.-X. Zhang, Y.-T. Hsu, and S. D. Sarma, arXiv preprint arXiv:1909.07980 (2019).
- [53] Z. Yan, *Phys. Rev. Lett.* **123**, 177001 (2019).
- [54] T. E. Pahomi, M. Sigrist, and A. A. Soluyanov, arXiv preprint arXiv:1904.07822 (2019).
- [55] S.-B. Zhang, W. Rui, A. Calzona, S.-J. Choi, A. P. Schnyder, and B. Trauzettel, arXiv preprint arXiv:2002.05741 (2020).
- [56] W. A. Benalcazar, J. C. Y. Teo, and T. L. Hughes, *Phys. Rev. B* **89**, 224503 (2014).
- [57] S. Ono, Y. Yanase, and H. Watanabe, *Phys. Rev. Research* **1**, 013012 (2019).
- [58] K. Shiozaki, arXiv preprint arXiv:1907.13632 (2019).
- [59] A. Skurativska, T. Neupert, and M. H. Fischer, *Phys. Rev. Research* **2**, 013064 (2020).

- [60] S. Ono, H. C. Po, and H. Watanabe, arXiv preprint arXiv:1909.09634 (2019).
- [61] M. Geier, P. W. Brouwer, and L. Trifunovic, arXiv preprint arXiv:1910.11271 (2019).
- [62] E. Roberts, J. Behrends, and B. Béri, arXiv preprint arXiv:1912.06609 (2019).
- [63] W. A. Benalcazar, T. Li, and T. L. Hughes, Phys. Rev. B **99**, 245151 (2019).
- [64] F. Schindler, M. Brzezińska, W. A. Benalcazar, M. Iraola, A. Bouhon, S. S. Tsirkin, M. G. Vergniory, and T. Neupert, Phys. Rev. Research **1**, 033074 (2019).
- [65] P. Zhu, K. Loehr, and T. L. Hughes, arXiv preprint arXiv:1910.10180 (2019).
- [66] We note that some models in Ref. [56] are actually 2d Kitaev superconductors.
- [67] Just to clarify, we always assume an equal number of atomic sites and pairs of electron and hole orbitals in our notation. So it is possible that some specific atomic site could be counted repeatedly in a special situation. For example, if a system has two pairs of electron and hole orbitals sharing the same atomic site, we will assume that there are actually *two* independent atomic sites that coincide at the same location. This one-to-one mapping between atomic site and its own electron orbital and hole orbital will greatly facilitate our later building-block construction.
- [68] R. Resta, Rev. Mod. Phys. **66**, 899 (1994).
- [69] I. Seroussi, E. Berg, and Y. Oreg, Phys. Rev. B **89**, 104523 (2014).
- [70] S. Liu, A. Vishwanath, and E. Khalaf, Phys. Rev. X **9**, 031003 (2019).
- [71] It should be emphasized that for fragile topological insulators, the term “fragile” is meant for both Wannier obstruction and band topology [73]. However, for a TSC with fragile Wannier obstruction, the fragility only occurs for the Wannier obstruction while its band topology could still be stable. Therefore, we will denote such systems “TSCs with fragile Wannier obstruction” instead of using the confusing term “fragile TSCs” that might have existed in some literatures.
- [72] A. Alexandradinata, X. Dai, and B. A. Bernevig, Phys. Rev. B **89**, 155114 (2014).
- [73] H. C. Po, H. Watanabe, and A. Vishwanath, Phys. Rev. Lett. **121**, 126402 (2018).
- [74] D. Vu, R.-X. Zhang, and S. Das Sarma, to appear.
- [75] F. Schindler, B. Bradlyn, M. H. Fischer, and T. Neupert, arXiv preprint arXiv:2001.02682 (2020).
- [76] N. Read and D. Green, Phys. Rev. B **61**, 10267 (2000).